Hybrid QPSO assisted Incremental Conductance MPPT Algorithm under Extreme Partial Shading Conditions

by

Quazi Rafid Hassan (170021085)
Sanzana Tabassum (170021125)
Imtiaz Mahmud Nafi (170021131)

A Thesis Submitted to the Academic Faculty in Partial Fulfillment of the Requirements for the Degree of

BACHELOR OF SCIENCE IN ELECTRICAL AND ELECTRONIC ENGINEERING

Department of Electrical and Electronic Engineering
Islamic University of Technology (IUT)
Gazipur, Bangladesh

May 2022

Certificate of Approval

The thesis titled 'Hybrid QPSO assisted Incremental Conductance MPPT Algorithm under Extreme Partial Shading Conditions' submitted by Quazi Rafid Hassan (170021085), Sanzana Tabassum (170021125), and Imtiaz Mahmud Nafi (170021131) of academic year 2020-21 has been found as satisfactory and accepted as partial fulfillment of the requirement for the Degree of Bachelor of Science in Electrical and Electronic Engineering.

Approved by:

Fahim Abid

Dr. Fahim Abid

Supervisor and Assistant Professor,
Department of Electrical and Electronic Engineering,
Islamic University of Technology (IUT),
Boardbazar, Gazipur-1704.

Date: 10. 05 .2022

Candidate's Declaration

It is hereby declared that this thesis or any part of it has not been submitted elsewhere for the award of any degree or diploma.

Signature of the Candidate

_____
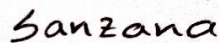QUAZI RAFID HASSAN
Student No.: 170021085
Session 2020-2021
Department of Electrical and Electronic Engineering (EEE)
Islamic University of Technology (IUT), OIC
Board Bazar, Gazipur
Dhaka, Bangladesh.

_____
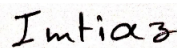SANZANA TABASSUM
Student No.: 170021125
Session 2020-2021
Department of Electrical and Electronic Engineering (EEE)
Islamic University of Technology (IUT), OIC
Board Bazar, Gazipur
Dhaka, Bangladesh.

_____
IMTIAZ MAHMUD NAFI
Student No.: 170021131
Session 2020-2021
Department of Electrical and Electronic Engineering (EEE)
Islamic University of Technology (IUT), OIC
Board Bazar, Gazipur
Dhaka, Bangladesh.

Acknowledgements

Table of Contents

List of Tables

List of Figures

List of Acronyms

PV   Photovoltaic

MPP   Maximum power point

MPPT   Maximum power point tracking

PSC   Partial shaded conditions

IC   Incremental conductance

P&O   Perturbation and observation

CS   Cuckoo search

PSO   Particle swarm optimization

QPSO   Quantum particle swarm optimization

PA   Proposed algorithm

STC   Standard test condition

PGS   PV generation system

PWM   Pulse width modulation

LMPP   Local maximum power point

GMPP   Global maximum power point

Abstract

Photovoltaic (PV) has seen rapid growth over the last decade because of its declining cost, minimal pollution, and easier maintenance. However, one major drawback of the PV systems is the non-linear characteristics of the output power caused by partial shading conditions (PSC). Varying weather phenomena, like temperature and solar irradiance, confront the PV with a multi-peak maximum power point tracking (MPPT) problem. To resolve this, many conventional and metaheuristic optimization MPPT algorithms have been proposed, some of which come with problems like slower tracking speed, increased oscillation, and no guarantee of accurate convergence at the global maximum power point (GMPP). This paper presents a hybrid quantum particle swarm optimization assisted variable incremental conductance (QPSOVIC) algorithm which efficiently tracks maximum power (P_{max}) under varying weather conditions. The effectiveness of this method is validated through a comparative analysis among already established MPPT techniques like cuckoo search (CS), particle swarm optimization (PSO), and QPSO. This metaheuristic algorithm compensates for the conventional tracking algorithm's inability to track the GMPP and bypasses premature convergence of the traditional PSO algorithm. MATLAB/Simulink has been used for modeling and demonstration of the proposed algorithm.

Chapter 1

Introduction

1.1   Overview

The decrease in fossil fuel reserves, environmental concerns, and the rising cost of fossil fuel-based electricity has led to renewable energy resources (e.g., wind, hydro, solar, etc.) gradually replacing the conventional generation methods. The growing popularity of solar energy makes it an excellent alternative to conventional methods of power generation. Harnessing solar energy requires conversion technologies like PV, concentrated solar power (CSP), solar heating and cooling (SHC), etc. The most popular conversion technology, PV has over 633.7 gigawatts of global cumulative capacity as of 2020 [1]. Although the PV generation system (PGS) is clean, sustainable and inexhaustible, harnessing solar energy using PV modules comes with its own challenges that arise from the inconsistency of partial shading conditions (PSC). Various MPPT algorithms are used to tackle problems that are associated with PSCs.

1.2   Problem Statement

Since the PV arrays present a nonlinear power–voltage (P–V) characteristics curve which fluctuates with the environmental conditions, primarily the temperature and irradiance, achieving MPPT in real-time is essential to maximize efficiency of the system. MPPT is a method that extracts the maximum power from the PV modules and transfers that power to the load so that the PGS operates at the highest efficiency. A DC-DC converter is used to create an intermediate connection between the load and the module that enables the system to make necessary changes for achieving MPP. The load impedance observed by the source is controlled by varying the duty cycle and the pulse width modulation (PWM) of the gate pulses to transfer the maximum power. The PSC can have a considerable impact on the PV array output power depending on shade patterns, system design, and bypass diodes. During facing PSC, the PV modules of the same string experience varying irradiance, resulting in nonlinear PV characteristics that exhibit multiple peaks. A local maximum power point (LMPP) and a global maximum power point (GMPP) are formed as a result of these numerous peaks (GMPP). To mitigate this issue multiple metaheuristic algorithms have been proposed. However, they often come with issues like slow tracking, increased oscillation before reaching steady-state, and no guarantee of convergence [2]. However, by combining complementary features of multiple MPPT algorithms, an improved tracking efficiency, tracking time and reduced oscillation can be achieved.

1.3　　　Literature Review

There have been proposals of many conventional algorithms for MPP tracking purposes, among which perturbation and observation (P&O) [3], incremental conductance (IC) [4] and hill-climbing [5] methods are used most commonly. The downfall of these conventional methods is that they only work well in conditions on constant temperature and uniform change in illumination. Under varying irradiance and temperature, it converges to one single MPP. After reaching the first maximum point (which might or might not be the GMPP), the algorithm stops advancing to the maximum points and gets trapped in a LMPP [6]. P&O technique often results in incorrect conclusion and oscillation before reaching the MPP. When solar irradiance fluctuates severely, the algorithm starts losing its direction towards the MPP [7]. The shortcomings of the P&O can be overcome by the IC. Although IC comes with its drawbacks, such as- power losses caused by oscillations near the MPP while reaching the steady-state (when used step size is large), slow convergence rate while tracking the optimal operating point (when used step size is small), and operating point may diverge from the MPP under varying meteorological conditions [8].

Later, some improvements were made to the conventional algorithms to enhance the MPPT ability during fast-varying irradiance level and load changes [9], [10]. To track the MPPT faster, a simple trigonometric rule has been applied for establishing a relationship between the IV curve and the load line [11]. A dynamic MPPT controller under rapidly changing conditions has been proposed in [12], where to determine the maximum output power capacity for a certain operating state, a scanning technique is used [13]. But like most conventional algorithms, when partial shading is introduced, both IC and P&O are not able to separate among the LMPP and GMPP. These techniques can only operate accurately in a single peak output characteristics, and the tracking is merely based on the positive or negative gradient [14].

According to the behavioral pattern of swarm movements of insects like ants, various bio-inspired techniques are designed for tracking the GMPP among multiple LMPPs. Some examples of metaheuristic techniques developed for MPPT are ant colony optimization (ACO) [15], cuckoo search (CS) [16], particle swarm optimization (PSO) [17],   grey wolf optimization (GWO) [13], flower pollination algorithm (FPA) [18], firefly algorithm (FFA) or colony of flashing fireflies [19], artificial bee colony (ABC) [20], bat algorithm (BA) [21], moth–flame optimization (MFO) [22] etc. There are various types of DC-DC converters for the conjunction of PV array and load to achieve MPPT, such as the boost converter, buck-boost converter, Ćuk converter, SEPIC, etc. [23]. In this paper, because of its simple design, convenient control settings, and better efficiency than any other step-up converter, the boost converter is utilized to deploy a functioning model of PV together with MPPT.

PSO adopts an iteration-wise process to obtain the operational point when the global MPP is discovered, and it is a common metaheuristic algorithm. Despite PSO showing greater chances to achieve the global peak under PSC, their convergence rate is slow and there is no guarantee that it

will converge to the optimal operating region. Characteristics like simple mechanism, the ability of parallel processing, and good probability of finding globally optimal solutions make PSO much suitable to control MPPT of PV systems under PSC, but it still has some shortcomings [24]. Traditional PSO may cause premature convergence during the searching process. Particularly, it is common for traditional PSO to fall into the local extreme points under severe PSCs. Moreover, the performance of PSO will usually decline late in the search [25].

1.4   Motivation

The relevant work observed so far states that PSO-based algorithms are well suited to track MPPT but still have room for improvement due to slow convergence and unpredictability of global convergence. The possibilities to reach global convergence can be ensured by eliminating the improper initialization and velocity update constraints. Hence, by modifying the basic PSO and QPSO, a hybrid IC-based QPSO algorithm has been proposed in this paper. The most common problem found in the PSO method is due to factors of randomness, that the particles exhibit erroneous movements that might not point to the MPP. QPSO updates the velocity only based on the factor of α which does not always converge to global optima. So, the modifications are made in QPSO by introducing IC for improving the searchability and making the process faster. Thus these mutations contribute high value while updating the particle's next position and convergence , and it is always achieved at the GMPP [26]. This study aims to deriving a hybrid QPSOVIC algorithm through combining the IC and stochastic-based quantum particle swarm optimization (QPSO) that exhibit superior characteristics in tracking and convergence compared to many of the existing algorithms.

1.5   Thesis Outline

Chapter 1 presents the general introduction and background of our study in a precise manner. Chapter 2 describes characteristics of PV system and boost converter. Chapter 3 consists of some highlighted conventional and metaheuristic. Chapter 4 will discuss about our proposed algorithm formation and simulation setup. Chapter 5 will consist of the experimental analysis and result comparisons. Finally, chapter 6 presents the conclusion and a brief discussion on future work.

Chapter 2

Characteristics of PV System and Converter

2.1 Basic model of a PV Cell

The equivalent circuit representation of a single PV cell is illustrated in Figure 2.1 that makes it easier to calculate the design parameters and visualize dynamic interaction between the device components. The configuration may consist of a single diode [27] or two diodes [28]. In this paper, the double diode configuration is being considered [29]. The PV cell consists of photo current (I_{ph}), series and parallel resistances (R_s, R_p) that take into consideration the resistive losses and two diodes (D_1 and D_2) whose inverse saturation current is entirely temperature dependent. For representing recombination currents everywhere, D_1 is used except for the space charge region. In that region, D_2 is used for model Shockley–Read–Hall recombination currents. For simplicity, as the shunt resistance R_p has a fairly high value and acts like an open circuit, thus it is neglected [30].

Table 2.1 Symbols and description of parameters of the PV system and boost converter

Symbol	Description
I	PV module output current (A)
I_{ph}	Photocurrent (A)
I_{sat_1} , I_{sat_2}	Saturation current of diodes D_1 and D_2 respectively (A)
n_1 , n_2	Ideality factor of diodes D_1 and D_2 respectively
N_s	No. of the series-connected cells in PV module
N_p	No. of the parallel-connected cells in PV module
R_s , R_p	Series and parallel/shunt resistance of the PV module (Ω)
V	PV module output voltage (V)
V_{th_1} , V_{th_2}	Thermal equivalent voltage of diode D_1 and D_2 respectively (V)
V_{in}	Input voltage of boost converter
V_{out}	Output voltage of boost converter
D	Duty cycle of boost converter
L	Inductance of boost converter
C_{in}	Input capacitance of boost converter
C_{out}	Output capacitance of boost converter
f_s	Switching frequency
ΔV_{ld}	Load ripple voltage of boost converter
ΔI_{id}	Inductor ripple current of boost converter
T_{on}	Total on period of the signal
T_{switch}	Total period of the signal
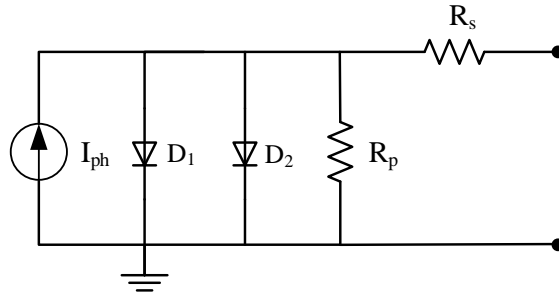
Figure 2.1 Equivalent circuit diagram of a double diode representation of a PV cell

There are some non-linearity factors associated with the PV output current-voltage (I-V) equation [31]. In this model we take it as linear [32] and calculate using the following equation:

$$I = I_{ph} - I_{sat\_1}\left[exp\left(\frac{V + IR_s}{n_1 N_s V_{th\_1}}\right) - 1\right] - I_{sat\_2}\left[exp\left(\frac{V + IR_s}{n_2 N_s V_{th\_2}}\right) - 1\right] - \left(\frac{V + IR_s}{R_p}\right) \quad (1)$$

The PV module selected for this study is 1Soltech 1STH 215-P PV module, and it can generate an output power of 213.15 W.

Table 2.2 Electrical Characteristics of 1Soltech 1STH 215-P PV module used in this study

Symbol	Parameter	Value
μ_{Isc}	Temperature coefficient of I_{sc}	.00102 A/°C
μ_{Voc}	Temperature coefficient of V_{oc}	-.0036099 V/°C
q	Charge of electron	1.6e-19 C
K	Boltzmann constant	1.38e-23 JK^{-1}
n	Diode ideality factor	.98117
E_{go}	Bandgap	1.1 eV
R_s	Series resistance	0.3938 Ω
R_p	Shunt resistance	313.3991 Ω
T_n	Nominal temperature	298K
V_{oc_stc}	Open circuit voltage	36.9 V
N_p	No. of module connected in parallel	4
N_s	No. of cells connected in series	60
I_{sc}	Short circuit current	7.84 A
V_{mp}	Voltage at MPP	29 V
I_{mp}	Current at MPP	7.35A
P_{mp}	Single module maximum power	213.15W

A single PV module produces limited output voltage and current, so to meet practical needs multiple PV modules need to be in series or parallel connections. For a PV module, the equation can be written as-

$$I = N_p I_{ph} - N_s I_{sat_1}\left[exp\left(\frac{(V + IR_s)}{n_1 N_s V_{th_1}} - 1\right)\right] - N_s I_{sat\_2}\left[exp\left(\frac{(V + IR_s)}{n_2 N_s V_{th\_2}} - 1\right)\right] - \frac{V + IR_s}{R_p} \quad (2)$$

2.2 PV cell Characteristics

A solar cell is considered ideal if the shunt (parallel) resistance (R_p) is enormous, and the series resistance (R_s) is very small. Compared to the forward resistance of a diode, R_p is much larger for commercially available solar cells. Under constant irradiance and temperature, Figure 2.2 illustrates the P-V characteristics of the PV cell. The peak parameters have been marked and observed so that the overall curve depends on V_{oc} and I_{sc} [33]. Under changing irradiance and temperature, the I-V characteristics are illustrated in Figure 2.3. The curve holds three significant parameters- short circuit current (I_{sc}), open circuit voltage (V_{oc}) and maximum power point (MPP). Intrinsic characteristics of the PV cell and external factors, mainly the temperature and the irradiation level control the I-V characteristics.
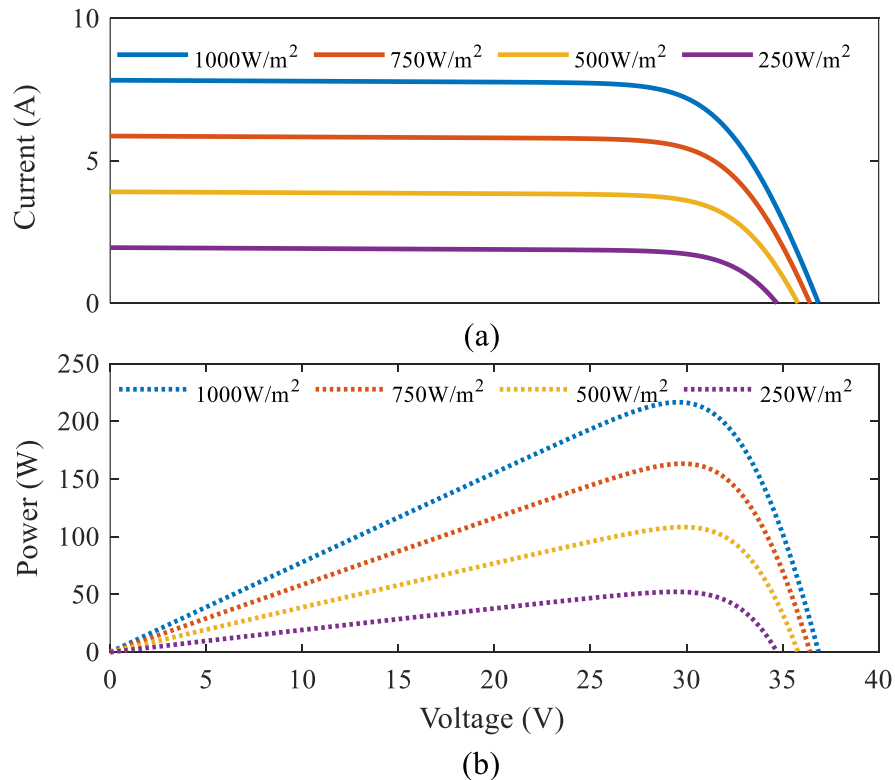
Figure 2.2 Effect of varying irradiance levels (a) I-V characteristics and (b) P-V characteristics of a PV module
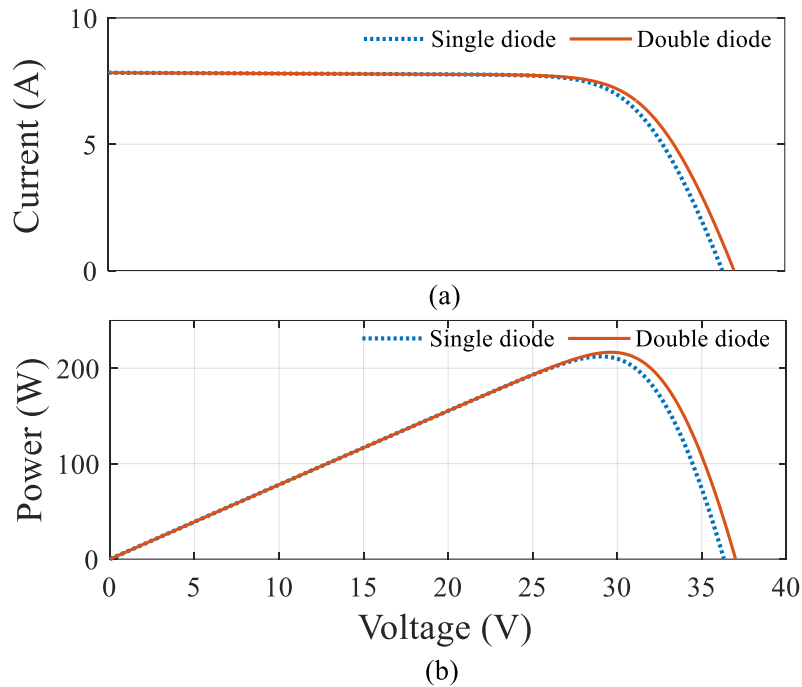
Figure 2.3 (a) P-V characteristics and (b) I-V characteristics of a PV module under uniform irradiance and temperature

From Figure 2.3, we discovered that the PV module shows a non-linear characteristic which changes depending on temperature, solar irradiance, and load condition. The varying conditions result in new characteristic curves, and each curve has a point on which maximum power can produced by the module. Here an MPPT controller is required for operating a highly efficient DC-DC converter that enables the module to work at its GMPP [34].

2.3   Effect of PSC on PGS:

Each module is exposed to variable external conditions such as non-uniform irradiation when series and parallel configurations are utilized in PV cells to provide appropriate output. The inconsistency experienced by each module directly affects the PV system output. During the cloudy days, the panels witness frequent and dynamic insolation differences while dusting accumulates those results in a gradual change in received insolation. During the periods of varying external factors, the panels that receive less irradiation are considered as the shaded modules. These shaded modules can serve as a load which instead of supplying power to the system, draws it from other modules. The excessive power dissipation creates hot-spot effects. Increasing the PSC increases the risk of damage to the panels owing to overheating issues, as well as lowering the system's efficiency. To mitigate this issue, a bypass diode is connected with each panel in the

PV array that gets forward biased in case of any irradiation change [35]. Introducing bypass diodes reduces the effect of overheating due to reverse bias. However, because of these bypass diodes, multiple peaks in P-V and I-V curves are generated, which can be observed in Figure 2.4. The U and P respectively stand for uniform and partial irradiance experienced by each module. 2U2P refers to 2 modules that experience uniform irradiance and 2 modules that sustain partial irradiance. The temperature is kept constant. The maxima on each P-V curve and the partially shaded modules are equal in number. Conventional algorithms are impotent to distinguish between LMPPs and GMPP that cause power loss and decreased efficiency [36]. Since, on the curves, multiple peak points are produced by PSC, there is a high compromise of the efficiency of these gradient-based algorithms. It is possible to locate the global maxima with the help of bio-inspired metaheuristic techniques in case of uniform irradiance also in PSCs and have been implemented successfully in MPPT applications.
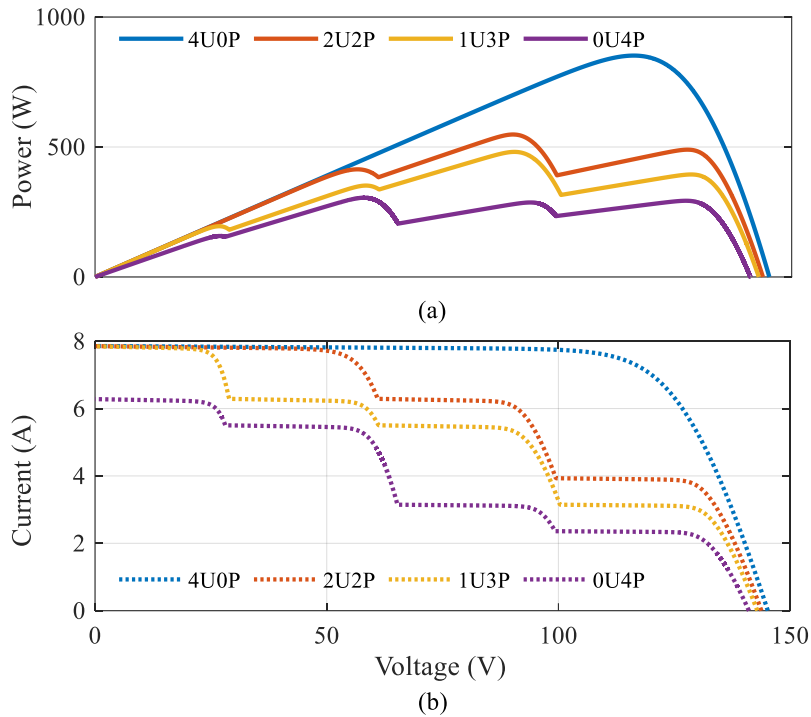
Figure 2.4 (a) P-V characteristics and (b) I-V characteristics of a PV module under partial shading condition

2.4 Boost Converter

The boost converter, a specific configuration of the DC-DC converter, plays an important role in the MPPT system and mainly serves two purposes. First, it works as an interface that connects the PV array and the load. Secondly, for the MPPT controller, it acts as the controlling component. Changing the PWM signal's duty cycle adjusts the boost converter output in such a way which enables the PV system to work at GMPP. The operational frequency, input-output voltages,

inductance, capacitance, and other electrical parameters are calculated using the following equations:

$$V_{out} = \frac{V_{in}}{1 - D} \tag{3}$$

$$D = \frac{t_{on}}{t_{switch}} \tag{4}$$

$$C_{in} = \frac{\Delta I_{id}}{8\Delta V_{ld}f_s} \tag{5}$$

$$L = \frac{V_{in}D}{2\Delta I_{id}f_s} \tag{6}$$

$$C_{out} = \frac{ID}{\Delta V_{ld}f_s} \tag{7}$$
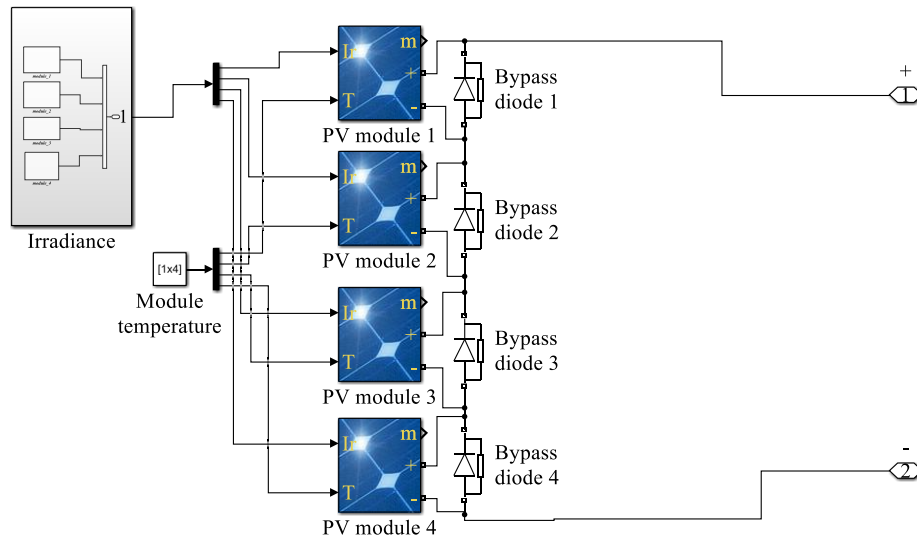
Figure 2.5 Schematic diagram of a basic PV system

To implement the newly proposed method, the generated PWM is fed into the gate of the DC-DC converter as the duty cycle [37].

Chapter 3

Conventional MPPT Algorithms

3.1   Cuckoo Search:

CS algorithm is modelled after the cuckoo birds' biological and reproductive behavior, which Yang Xinshe and Deb Suash have proposed [38]. Observation shows that for laying eggs, various species of cuckoos use nests of other birds' (host birds), which is referred to as brood parasitism [39]. Cuckoos follow different strategies to increase their reproduction probabilities, such as imitating the color and shape of the host birds' eggs, maintaining timing of laying eggs, proper selection of host nests with similar egg characteristics, destroying some of the host birds' eggs etc. Managing to differentiate the cuckoo's eggs is a common phenomenon for the host birds as well. Host birds then destroy those eggs or completely abandon the nest and go somewhere else for building a new nest [16]. This is why cuckoos follow certain techniques to maximize the chances of their eggs surviving.

Searching for a proper nest can be compared to searching for food. This is observed in a random or a quasi-random form. Based on certain mathematical functions during exploration of foods, trajectories or directions chosen by animals can be modeled. Depending on cuckoos' brood parasitic behavior, three idealized rules are presented by Yang and Deb [38]: (1) per iteration, each cuckoo lays one egg, and it is placed in a nest that is selected randomly, (2) the best nest having eggs of the highest quality would be carried forward to the future generation and (3) total number of nests available is constant, and host bird finding the cuckoo's egg has a probability of P_a, where $0 < P_a < 1$.

For a cuckoo, the following equation performs a Lévy flight, while yielding a new solution $x^{(t+1)}$:

$$x_i^{(t+1)} = x_i^t + \alpha \oplus Lévy(\lambda) \tag{8}$$

where the samples(eggs) are denoted by x_i^t, sample number by i, iteration number by t and the step size by $\alpha > 0$. The product $\oplus$ indicates entry-wise multiplication. α is mostly used as,

Start

Initialize the parameters

Sense V,I; Randomly generate 'n' samples

Calculate power; Find current best voltage V_best^t

Obtain next generation using Levy flights;
$v_i^{(t+1)} = v_i^t + \alpha \oplus Lévy(\lambda)$

Obtain new fitness array $[J]^{t+1}$ and find current best voltage V_best^{t+1}

If any element of $[J]^{t+1} > [J]^t$ No

Yes

Best voltage = V_best^{t+1} Best voltage = V_best^t

t+1   t+1

No   Max_iter?

Yes

Yes   Change in irradiation
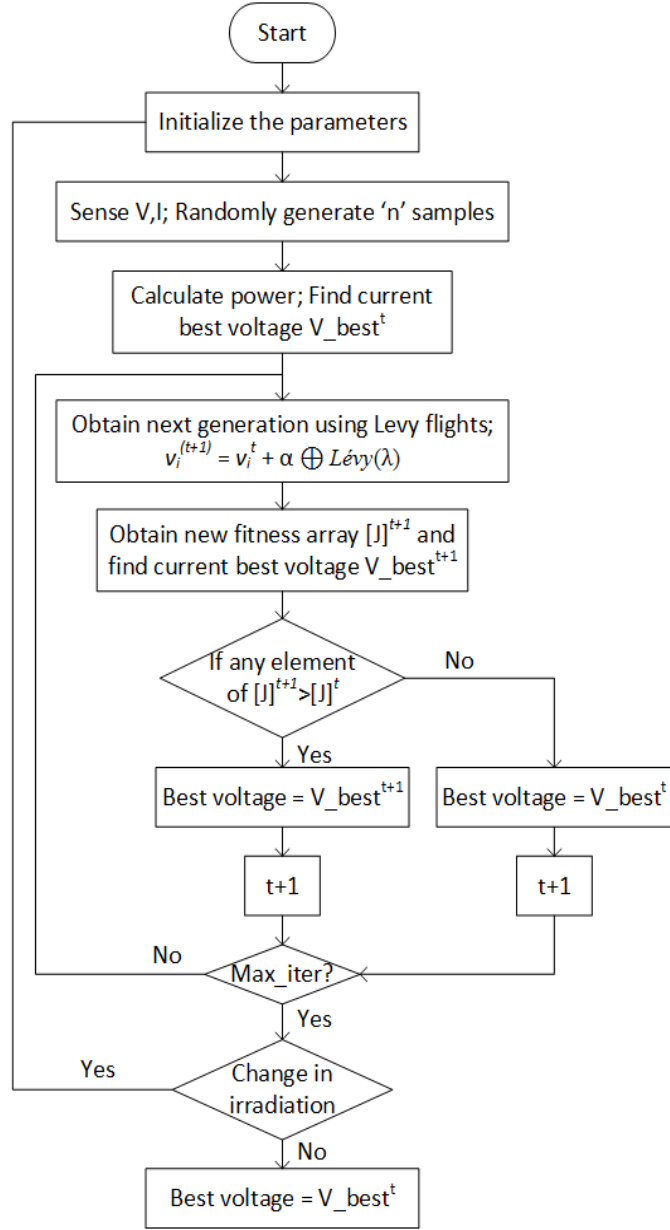
No

Best voltage = V_best^t

Figure 3.1 Flowchart of CS algorithm

$$\alpha = \alpha_0(x_j^t - x_i^t) \tag{9}$$

where α_0 is the Lévy multiplying coefficient and $x_j^t - x_i^t$ is the difference between two samples. In [40], a simpler process of Lévy distribution is given as:

$$s = \alpha_0(x_j^t - x_i^t) \oplus L\acute{e}vy(\lambda) \approx \kappa \times \left(\frac{u}{(|v|)^{\frac{1}{\beta}}} \right)(x_j^t - x_i^t) \tag{10}$$

where β=1.5 and the normal distribution curves give u and v:

$$u \approx N(0, \sigma_u^2) \tag{11}$$
$$v \approx N(0, \sigma_v^2) \tag{12}$$

If the integral gamma function is denoted by Γ, then,

$$\sigma_u = \left(\frac{\Gamma(1 + \beta) \times sin(\pi \times \beta/2)}{\Gamma\left(\frac{1 + \beta}{2}\right) \times \beta \times 2^{\left(\frac{\beta-1}{2}\right)}} \right)^{1/\beta} \tag{13}$$

$$\sigma_v = 1 \tag{14}$$

The respective power is measured for the new voltage samples. In order to get the new best sample, the P_{max} is selected by analyzing all the power values. Apart from the best sample, the remaining samples are destroyed randomly with a probability of P_a. For replacing the destroyed ones, new samples are generated randomly. Respective power of every sample is noted and the highest power is chosen. Until every sample reaches the MPP, this process is repeated.

3.2 Incremental Conductance

IC is a very popular conventional MPPT algorithm which uses the simple principle that with respect to voltage, the derivative of power at the MPP is zero ($dP/dV = 0$) [41]. The PV output power is, $P= VI$ where V and I are respectively the PV array output voltage and current. Differentiating it with respect to V we get,

$$\frac{dP}{dV} = \frac{d(V \times I)}{dV} = I + V \times \frac{dI}{dV} \Rightarrow \frac{1}{V} \times \frac{dP}{dV} = \frac{I}{V} + \frac{dI}{dV} \tag{15}$$

This algorithm has a simple approach of tracking the MPP by a gradient comparison method. At MPP the PV array power curve slope is zero. The slope increases to the left of MPP and decreases to the right. At MPP, $dP/dV=0$; so from equation, the conditions can be expressed as:

$$\frac{dI}{dV} = -\frac{I}{V} \quad (at\ MPP) \tag{16}$$

$$\frac{dI}{dV} > -\frac{I}{V} \quad (at\ left\ of\ MPP) \tag{17}$$

$$\frac{dI}{dV} < -\frac{I}{V} \quad (at\ right\ of\ MPP) \tag{18}$$

Using these three conditions, the incremental conductance algorithm flowchart can be illustrated like Figure 3.2.
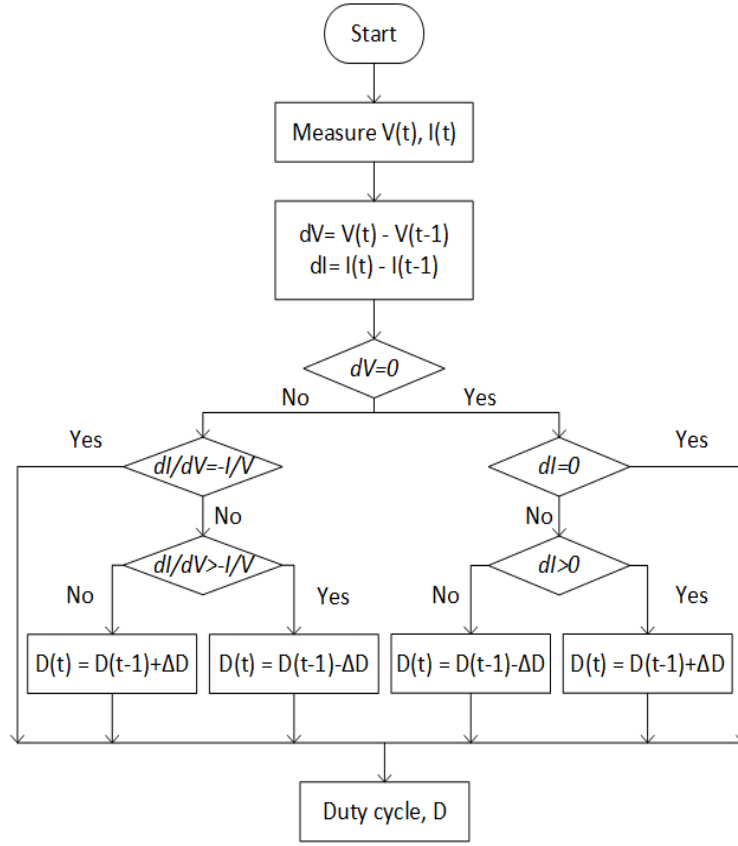
Figure 3.2 Flowchart of IC algorithm

3.3   PSO Algorithm

PSO is a stochastic, swarm intelligence based optimization algorithm, following the behavioral characteristics of bird flocks [17]. It evaluates a swarm of individuals (referred to as particles), where a probable solution is represented by each particle. The particle exchanges information it obtained from its own search process. Particles are guided by a simple strategy: compare the success of its evaluation to that of neighboring particles. In every iteration, the particles move under the influence of its own inertia, P_{best} which is the personal best solution, and also G_{best} which is the best solution in the neighborhood to locate the optimized solution. Until the terminating point is achieved, the particles update their orientation towards the optimal solution.

Updating the velocity and the positions of a particle of conventional PSO is represented mathematically as,

$$v_i(k+1) = wv_i(k) + x_i(k) + c_1 r_1 \left(P_{best(i)} - x_i(k) \right) + c_2 r_2 (G_{best} - x_i(k)) \qquad (19)$$

$$x_i(k+1) = x_i(k) + v_i(k+1) \qquad (20)$$

Where x_i represents the particle position which depends on the velocity component, v_i (representing the step size). The velocity is measured using inertia weight w; acceleration coefficients c_1, c_2, and random coefficients r_1, r_2, distributed uniformly from 0 to 1. $P_{best(i)}$ denotes the personal best position observed by particle i, and G_{best} denotes the overall best position observed by all the particles.

3.4 QPSO

Some improvement to the conventional PSO has been made by incorporating quantum mechanics and trajectory analysis of the PSO algorithm, resulting in a version of quantum-behaved PSO (QPSO) [42].

This algorithm reduces the number of parameters, giving it a better global optimization ability compared to the conventional PSO algorithm. Trajectory analysis [43] demonstrated that PSO can converge more accurately if each particle is converged to its local attractor, $LA_i^t = (la_{i1}^t, \ldots la_{id}^t \ldots, la_{iD}^t)$ where la_{id}^t is defined as follows [44],

$$la_{id}^t = \frac{c_1 r_1 pbest_{id}^t + c_2 r_2 gbest_d^t}{c_1 r_1 + c_2 r_2} \tag{21}$$

$$or, \quad la_{id}^t = \varphi pbest_{id}^t + (1 - \varphi) \, gbest_d^t \tag{22}$$

where $\varphi \in U(0,1)$, t is the current iteration number, $pbest_i$ is the best historical position found by particle i, and $gbest_i$ is the current global best position observed by the swarm.

In QPSO, to update the position of particle i and iteration t, Monte-Carlo method is used, resulting in an improved version of the iterative equation:

$$x_{id}^{t+1} = \begin{cases} la_{id}^t + \alpha|la_{id}^t - x_{id}^t| * ln\left(\frac{1}{u}\right), & r \geq 0.5 \\ la_{id}^t - \alpha|la_{id}^t - x_{id}^t| * ln\left(\frac{1}{u}\right), & otherwise \end{cases} \tag{23}$$

Where, $u \in U(0,1)$. The contraction–expansion coefficient $\alpha \in R^+$. To balance the overall searching ability of QPSO, the value of α can be assumed as $\alpha = 0.5 + 0.5 \, (T - t)/T$, where T and t represent the maximum and current number of iterations respectively.

The iteration process is done with (23) where the contraction–expansion coefficient α is the only parameter that needs to be adjusted. This limits dependence of the parameters on QPSO and the particle's speed does not affect the particle voltage. In addition, the small value of u results in a large value of ln(1/u) because of the quantum nature of particles (1/u). This makes jumping off the peak of the LMPPs easier for the particle, and searching around to reach the GMPP [42].
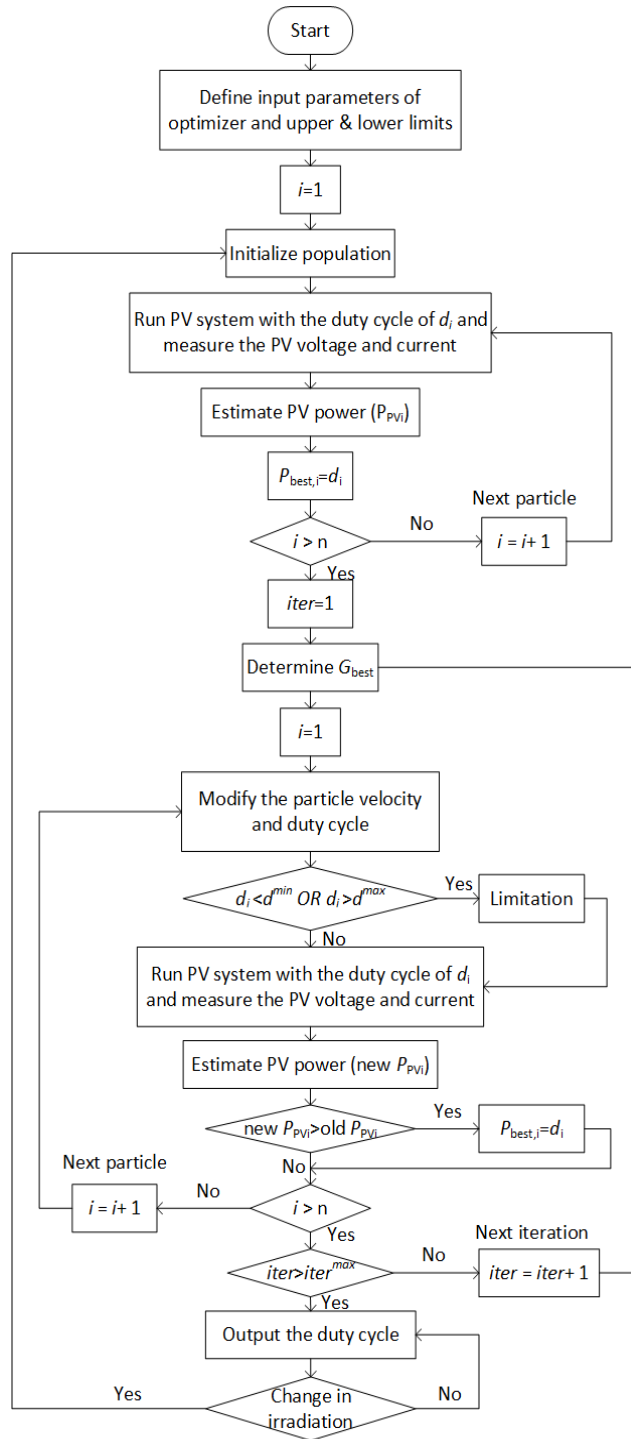
Figure 3.3 Flowchart of QPSO algorithm

Chapter 4

Methodology and Development of Experimental Setup

4.1 Formulating the hybrid algorithm

Despite incremental conductance popularity on conventional MPPT algorithm, it fails as regards tracking MPP under PSCs where a GMPP exists along with multiple LMPPs. Usually, it gets stuck tracking one of the LMPPs and never reaches the GMPP, and thus efficiency is significantly decreased [45]. To mitigate these problems, the necessity for a more accurate MPPT algorithm arises. The proposed hybrid quantum particle swarm optimization-based variable step size incremental conductance (QPSOVIC) algorithm combines the best characteristics of both QPSO and IC while excluding their shortcomings. A checking algorithm, QPSO, is generally implemented into the IC with a configurable step size in the suggested technique. Because it utilizes fewer tuning parameters than other algorithms, QPSO is used to locate GMPP. This makes it easier to implement in terms of hardware. It is easier to generate the boost converter duty cycle with higher accuracy in tracking global peak and reduced steady-state power fluctuation.

The main shortcoming of QPSO that the proposed algorithm will mitigate is the tracking speed. QPSO works by updating the velocity of the particles by exchanging their P_{best} and G_{best} after every iteration Figure 5.7(a). But once the GMPP has been located, there is no need to compare the P_{best} after every iteration (because G_{best} has already been found). Conventional QPSO continues to iterate by exchanging information between the particles until GMPP is reached, which slows down the rate of convergence. In the proposed algorithm, as soon as the GMPP is detected, the particles will break out of the iteration of QPSO and the operation of the IC algorithm will take place that will result in higher accuracy and better speed by operating at the GMPP detected previously.

The major drawbacks of conventional fixed size IC are higher tracking time and oscillation near MPP though it has good performance. To mitigate this issue several studies have proposed variable step size IC [9], [46]–[51]. In our study we used adjustment coefficient N(t) which gives larger step size far from MPP and smaller step size near MPP and also decreased tracking time.

$$N(t) = 1 + \left(\frac{V}{I} * \frac{dI}{dV} \right) \tag{24}$$

Instantaneous resistance is expressed by V/I, and incremental conductance is expressed by dI/dV. According to (16) (V/I) x (dI/dV) is a negative quantity and it continuously decreases as it reaches the MPP. The sharp change of (dI/dV) occurs on the right side of the MPP which is also mitigated using two initial perturbation step sizes. The duty cycle is updated according to the following equation-

$$D(t) = D(t-1) \pm N(t) * D_{ref} \tag{25}$$

$$D_{ref} = \begin{cases} D_{ref1} & D < D_{mpp} \\ D_{ref2} & D > D_{mpp} \end{cases} \tag{26}$$

We also use a power balance condition for initiating the variable step size IC algorithm. The equation is described as-

$$\Delta P(\%) \geq \frac{|P_{new} - P_{old}|}{P_{old}} \tag{27}$$

Complete process of the QPSOVIC is shown using the flowchart in Figure 4.1. For evaluating the performance of this algorithm based on tracking the GMPP under different shading patterns, MATLAB/Simulink was used to perform modeling and simulation. The test parameters used to check different PSCs are given in Table 2.2.

The proposed QPSOVIC algorithm has been simulated under different PSCs. In QPSOVIC, the duty cycle of the DC-DC converter used in the model that terminates the PI control loop is indicated by the position of a particle [52]. This simplifies the design of the controller and mitigates the complex computational load while tuning the gain of the controller.
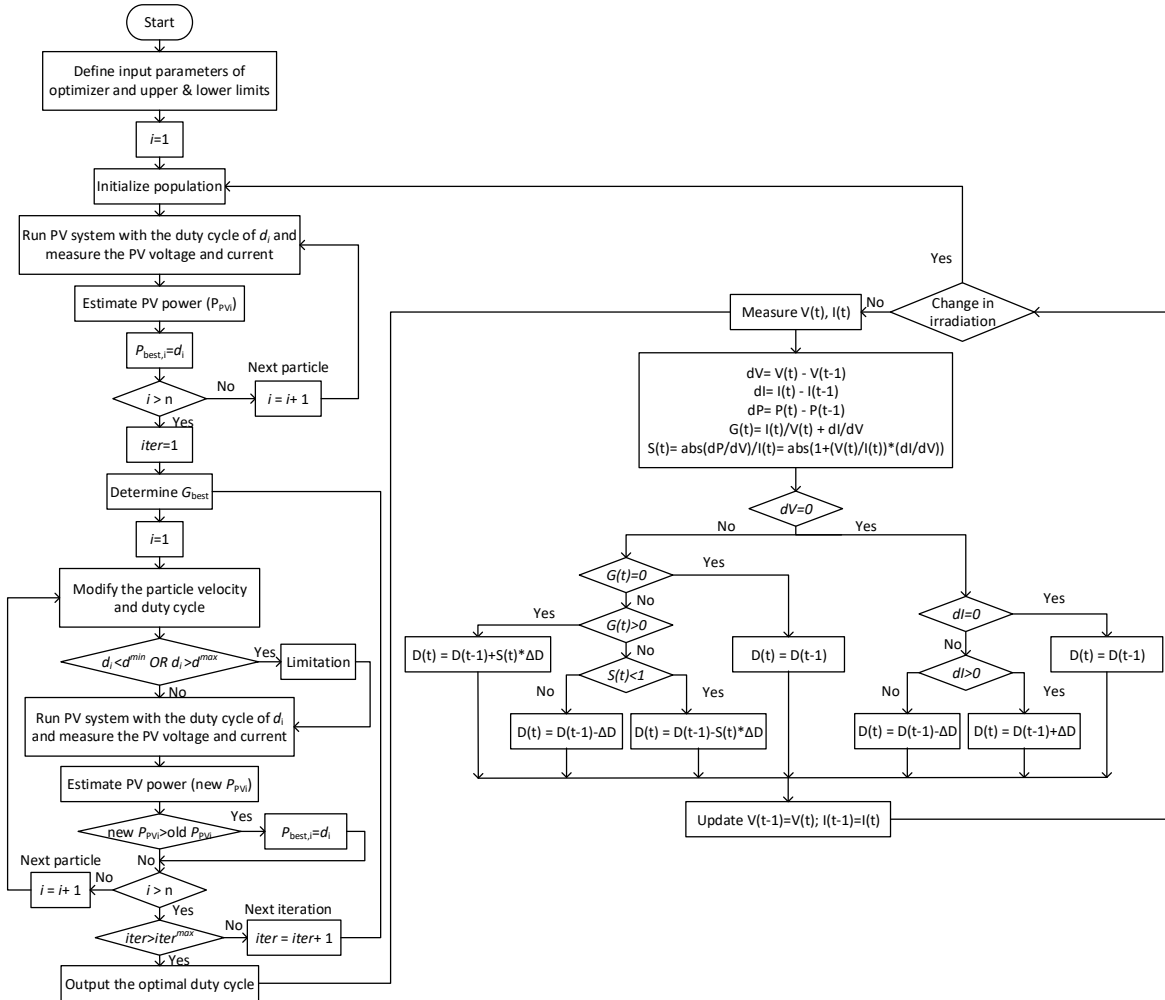

Figure 4.1 Flowchart for QPSOVIC algorithm

4.2 SIMULATION SETUP

The proposed QPSOVIC algorithm has been modeled and simulated using MATLAB Simulink for studying the system behavior and MPPT characteristics. Its performance has been compared with various metaheuristic algorithms like PSO, QPSO and CS. The block diagram in Figure 4.2 shows the total PV system with MPPT algorithm which feeds the duty cycle to a boost converter and power is supplied to a resistive load. In Table 4.1, the boost converter specifications are given. In the simulation, $C_1 = 1.2$, $C_2 = 1.2$, w = 0.4 are considered for tuning the PSO and the tuning parameter α is varying from 1 to .5 with every iteration where the maximum number of iterations is 200 (for QPSO). For comparison with CS, the random parameter P_0 is taken as 0.25 and the levy multiplying coefficient is 0.8. In the case of the proposed algorithm QPSOVIC, equation (27) is used to locate the GMPP and $\Delta P(\%)$ is set to 0.5 and $D_{ref2} = 10^{-5}$ where, $D_{ref1} = 3 * D_{ref2}$. Higher number of populations increases the computational complexity so we used four populations/particles to carry out this simulation.
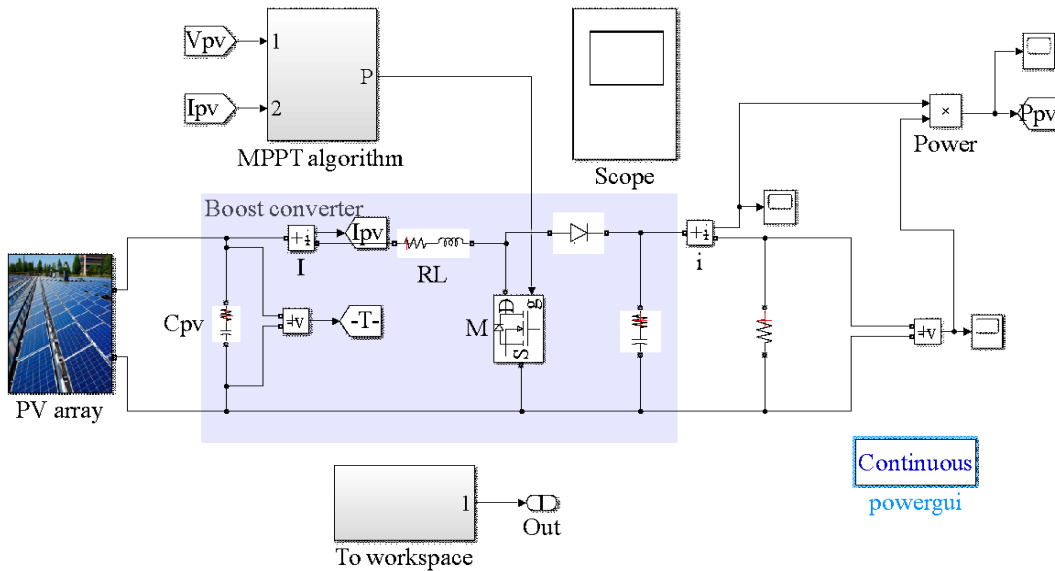

Figure 4.2 Simulation of PV system with hybrid MPPT

Table 4.1 DC-DC converter parameters

PV Link capacitor C_{pv}	100e-6 F, .001 ohm
Boost inductor L_{boost}	5e-3 H, 0.001 ohm
Boost Capacitor C_{boost}	437.5e-6 F , 0.0001 ohm
Load R_{load}	53 Ω
Frequency f_{boost}	50 KHz

The mathematical model is modelled with the photovoltaic panel 1Soltech 1STH 215-P in MATLAB Simulink. In Table 2.2, under the formulated test conditions, the specification and performance parameters of this PV model are given. The I-V curves and P-V curves for the built model under different irradiances and constant temperature (25°C) is given in Figure 2.3. The proposed QPSOVIC algorithm is simulated under different shading patterns where the irradiance is varied from 300 W/m^2 to 1000 W/m^2 and 25°C constant temperature is kept. The PV model has 4 modules, each of them experience a different irradiance under different test conditions. The test conditions are referred to as- 4U2P (4 uniform 0 partial), 2U2P (2 uniform 2 partial), 1U3P (1 uniform 3 partial), and 0U4P (0 uniform 4 partial), where U stands for uniform irradiance experienced by the module and P stands for partial irradiance experienced by the module. The corresponding electrical parameters are described in Table 4.2. From the table, it can be observed that the model exhibits multiple LMPPs across the modules subjected to PSCs and the overall system has one GMPP. To extract the available MP, the PV system must be operated at GMPP.

Table 4.2 Specification of irradiance and temperature for test conditions

Test Name	Module1 Irradiance	Module2 Irradiance	Module3 Irradiance	Module4 Irradiance	Cell temper-ature (C)	Voltage at MPPT (V)	Current at MPPT (A)	Power at MPPT (W)	No of peaks
4U0P	1000	1000	1000	1000	25	116.05	7.34	851.42	1
2U2P	500	800	1000	1000	25	90.07	6.08	547.84	3
1U3P	400	700	800	1000	25	90.3	5.33	481	4
0U4P	300	400	700	800	25	57.9	5.26	304.85	4

Chapter 5
Results

For different irradiances during PSCs, resultant I-V curves are given in Figure 2.4(b). With help of the resultant I-V curves, P-V characteristics are calculated and shown in Figure 2.4(a) [45], [53]. While carrying out the simulation, 25°C constant temperature was kept and different partial shaded conditions were used. The following subsections describe the results for each test condition.

5.1   4U0P Configuration:

In the first test condition 4U0P, four series connected PV modules are used which all are under uniform irradiance (Table 4.2). Under this configuration, there is only one MPP, so there is no need to track LMPP and GMPP explicitly. Under this test condition all the simulated algorithms have high efficiency and the tracking time is less than one second, QPSOVIC being significantly faster than PSO and QPSO Table 5.1. Also no algorithm fails to track the MPP because there is no chance of getting stuck in local maxima. The average current is traced at 7.15 A, 7.15 A, 7.31 A and 7.36 A by PSO, QPSO, CS and QPSOVIC respectively as shown in Figure 5.1. The average voltage is tracked at 118 V, 122.1 V, 116.4 V and 115.5 V by PSO, QPSO, CS and QPSOVIC respectively. In terms of efficiency, CS is on top with 99.9% and it is quickly followed by the proposed algorithm having 99.84%. Figure 5.2 and Figure 5.3 illustrates a zoomed view of power and duty cycle where the oscillation for QPSOVIC is much less than PSO and QPSO which results in the increased efficiency of QPSOVIC. The performance ranking can be made in terms of both efficiency and tracking time is CS > QPSOVIC > QPSO > PSO.
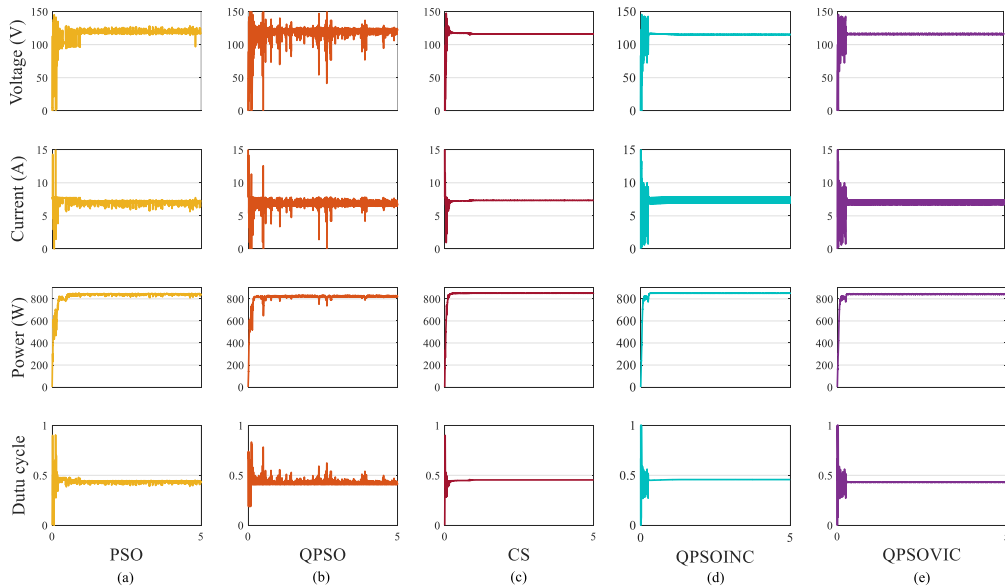

Figure 5.1 5 s simulation under 4U0P test condition for (a) PSO (b) QPSO (c) CS (d) QPSOINC (e) QPSOVIC
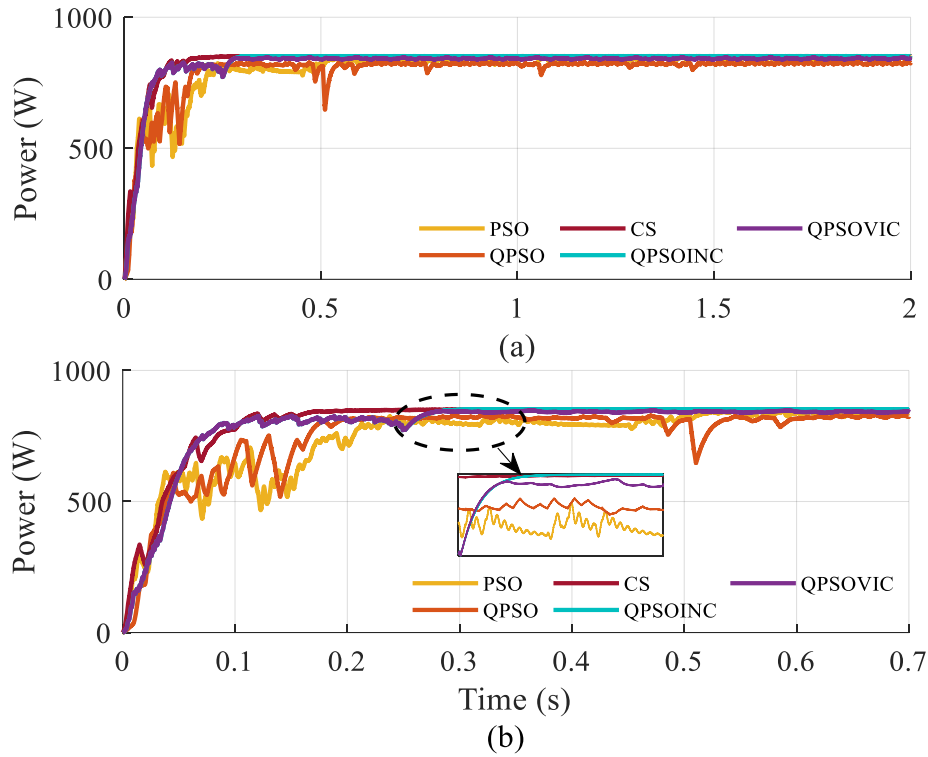
Figure 5.2 Power performance under 4U0P condition for (a) 5s (b) 0.6s (zoomed view)
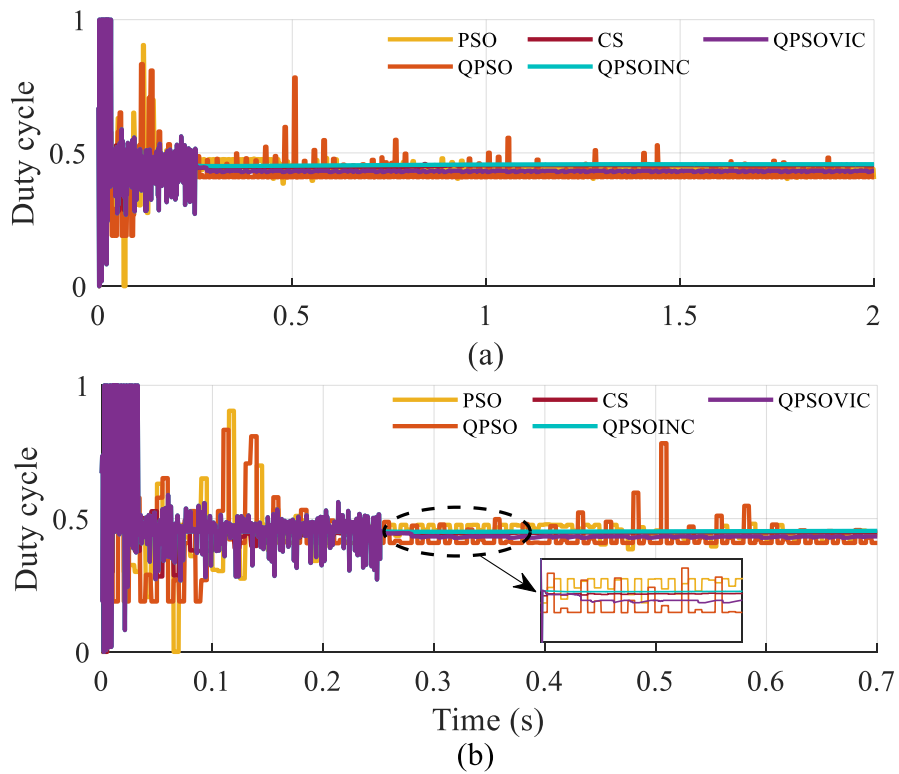

Figure 5.3 Duty Cycle under 4U0P condition for (a) 5s (b) 0.6s (zoomed view)

5.2   2U2P Configuration:

The 2U2P PV configuration exhibits two LMPPs and one GMPP. The corresponding powers from the LMPPs are 413.8 W and 489.6 W while the highest power at the GMPP is 547.84 W. Under this test condition all the simulated algorithms have high efficiency and the tracking time is less than one second. For this test case, the steady state power, average current, voltage and duty cycle are given in Figure 5.4 where CS and QPSOVIC have zero steady state oscillations. The transient power fluctuation is shown in Figure 5.5. The Pmax achieved by QPSOVIC is 547.82 W as compared to 532.8 W, 543.9 W and 545.7 W achieved by PSO, QPSO and CS. Average power over maximum power ratio gives the overall efficiency. PSO has the lowest efficiency of 96.97% and QPSOVIC exhibits highest efficiency of 99.99% and oscillation is much less compared to QPSO and PSO as shown in Table 5.1.
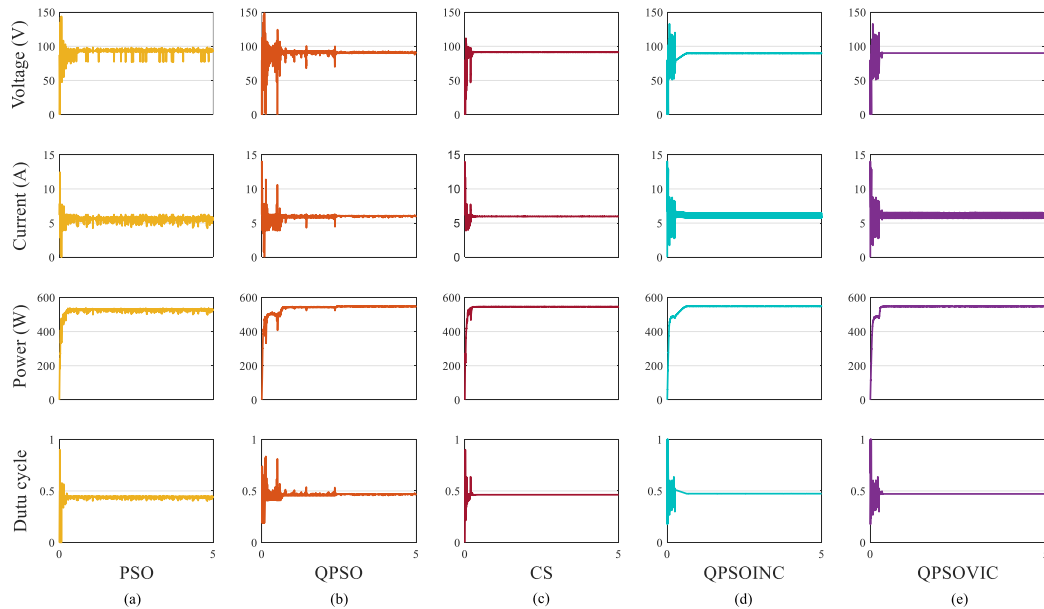
Figure 5.4 5 s simulation under 2U2P test condition for (a) PSO (b) QPSO (c) CS (d) QPSOINC (e) QPSOVIC

In terms of tracking time, QPSO takes the longest 0.69s s to reach the steady-state. The duty cycle of QPSOVIC gets saturated 0.65s which means it reaches GMPPs faster than QPSO as shown in Figure 5.6. The QPSOVIC works such that the QPSO feeds the boost converter duty cycle until it satisfies the convergence condition $\Delta P(\%) = 0.5$, which can be observed in Figure 5.7(a). The optimal duty cycle is calculated using equation (24) which is given as an initial condition to IC and it locates the GMPP with high accuracy and a fast-tracking period as shown in Figure 5.7(b). The ranking of the algorithm can be made in terms of efficiency and tracking time sequentially as QPSOVIC > CS > QPSO > PSO and CS > PSO > QPSOVIC > QPSO.

Figure 5.5 Power performance under 2U2P condition for (a) 5s (b) 0.6s (zoomed view)

Figure 5.6 Duty Cycle under 2U2P condition for (a) 5s (b) 0.6s (zoomed view)
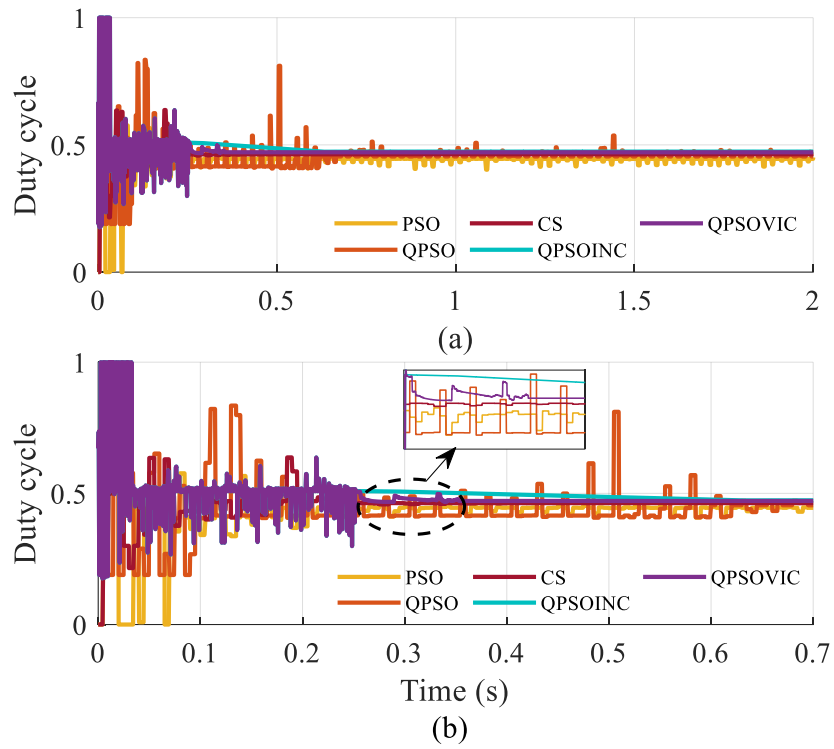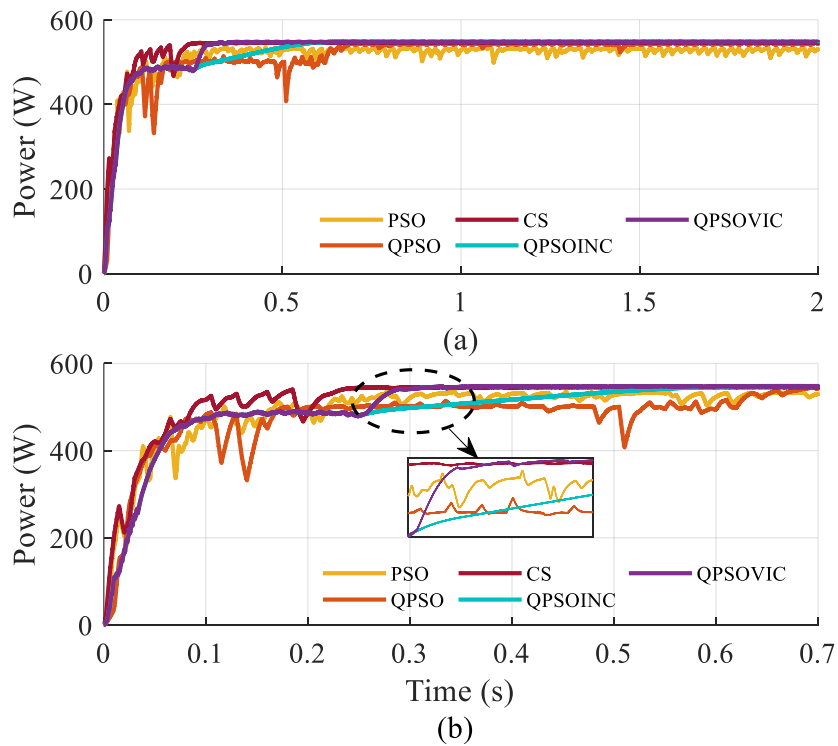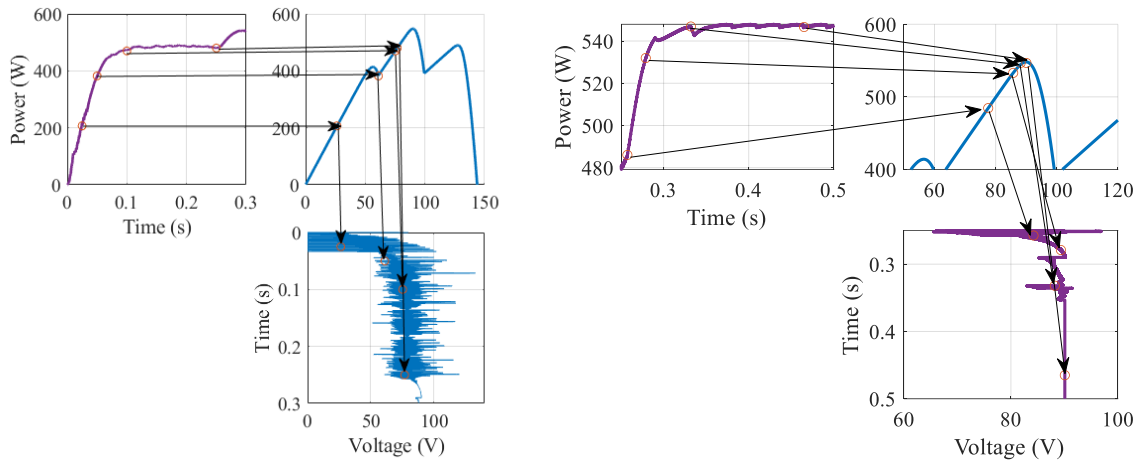
Figure 5.7 (a) Power climbing in partial shading 2U2P QPSO (b) Power climbing in partial shading 2U2P Variable step size IC

5.3   1U3P Configuration:

Test configuration 1U3P stands for 1 uniform and 3 PSCs experienced by the modules. This configuration exhibits three LMPPs and one GMPP Table 4.2. The corresponding powers from the LMPPs are 351.6 W, 393 W, and 195.2 W. The P_{max} observed at GMPP is 481 W. QPSO performs poorly in detecting the average current, whereas QPSOVIC tracks just at 5.33 A as shown in Figure 5.8. The voltage is also tracked inaccurately by PSO and QPSO, whereas CS and QPSOVIC manage to track it accurately. All the simulated algorithms exhibit high efficiency and tracking time of less than one second. PSO requires the highest tracking time of 0.9s to reach the steady-state. However, this configuration has lower efficiency compared to QPSO because of increased oscillation. The QPSOVIC has 99.98% efficiency and the tracking time is 0.3s which means IC is proved faster for tracking the peak. Like the previous scenario, the QPSO works by operating under QPSO in the first half of the algorithm and later transfers the optimal duty cycle as an initial condition to the IC algorithm. CS exhibits superior results with a tracking time of 0.26s. The current and voltage graphs are plotted in Figure 5.8, Figure 5.9 and Figure 5.10 show the detailed plot of the power and duty cycle. The performance comparison is CS > QPSOVIC > PSO > QPSO.
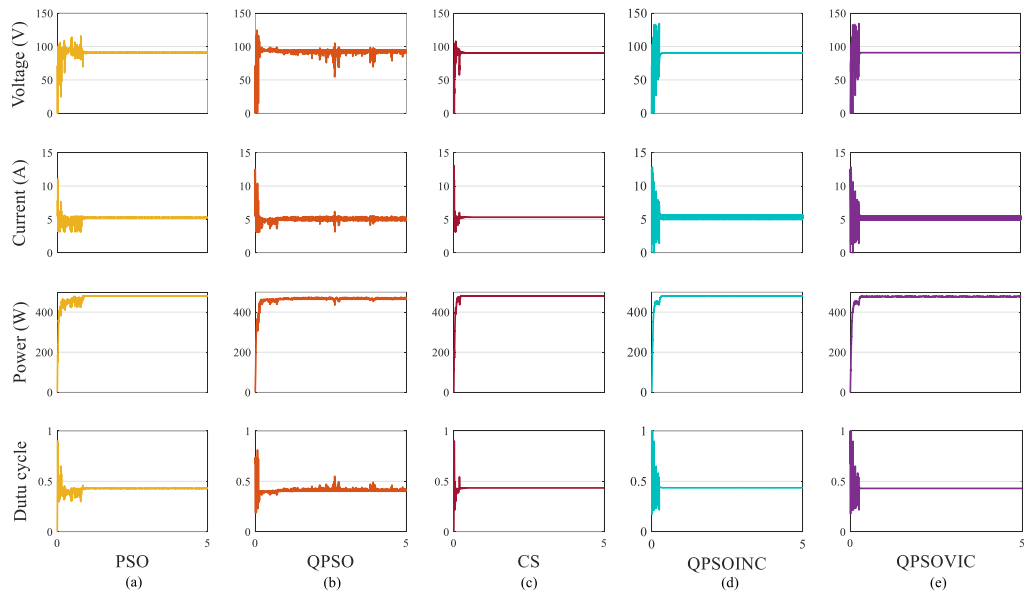
Figure 5.8 5 s simulation under 1U3P test condition for (a) PSO (b) QPSO (c) CS (d) QPSOINC (e) QPSOVIC
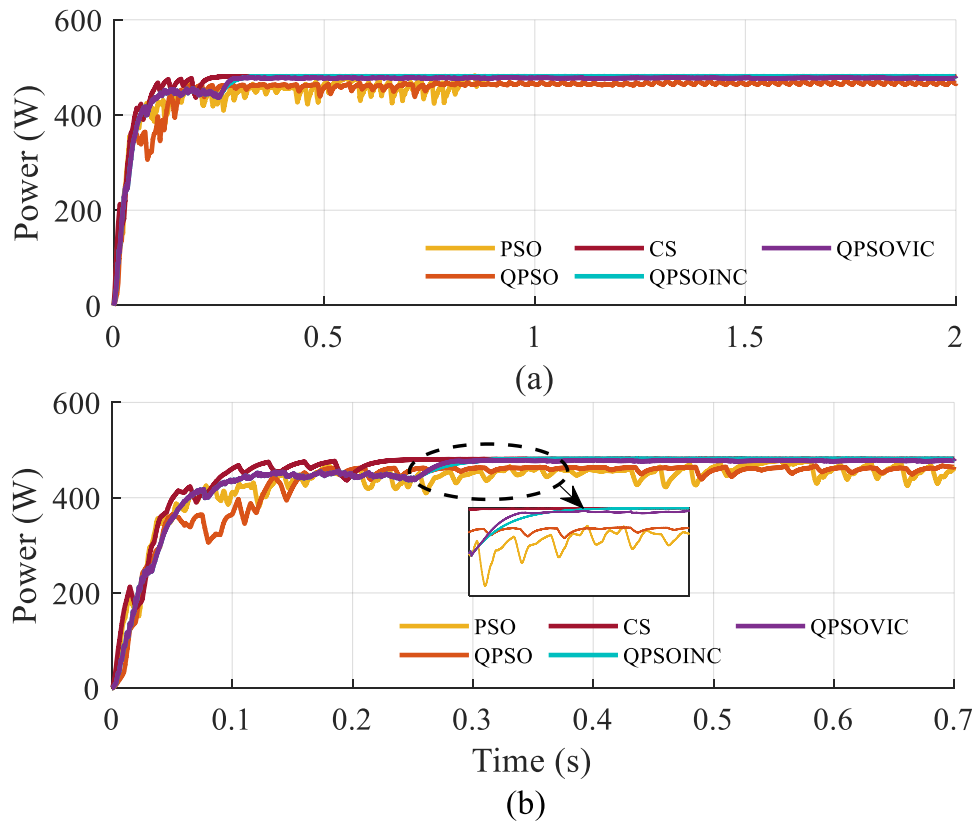

Figure 5.9 Power performance under 1U3P condition for (a) 5s (b) 0.6s (zoomed view)
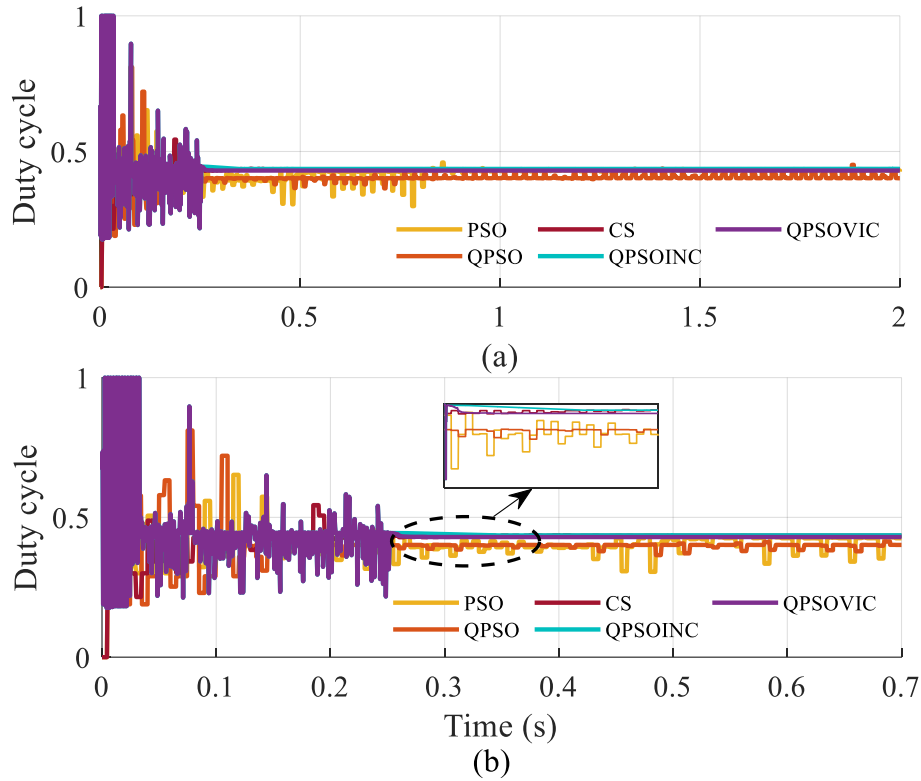
Figure 5.10 Duty cycle under 1U3P condition for (a) 5 s (b) 0.6 s (zoomed view)

5.4 0U4P Configuration:

All PV modules are under varying PSCs in this configuration. This configuration exhibits three LMPPs and one GMPP Table 4.2. The corresponding powers from the LMPPs are 157.7W, 286.6W and 290.4W. The P_{max} observed at GMPP is 304.8 W. PSO's failure to track GMPP under extreme PSCs can clearly be observed under this scenario. PSO algorithm completely diverges from the GMPP which is noticed in Figure 5.11. QPSO is used to mitigate this uncertainty of convergence. After searching the whole search area, QPSO locates the GMPP and calculates the optimal duty cycle. This optimal duty cycle is passed on to the IC algorithm which quickly converges to GMPP. QPSOVIC gets the highest power 304.7 W and PSO tracks an LMPP which can be observed in Figure 5.12. Although QPSO can assure convergence, it is less accurate in determining the average current and maximum voltage of the system. CS and QPSOVIC both track the current and voltage more accurately. In terms of tracking time, QPSOVIC is much faster than QPSO with 0.43s, but CS is the fastest to track it under 0.3s which is seen in Figure 5.13.On the contrary, QPSOVIC shows the highest efficiency of 99.95% out of all four algorithms, leaving behind CS (99.79%), QPSO (99.29%), and PSO (88.14%). These outcomes highlight the QPSOVIC's assured convergence and highest efficiency under extreme PSCs that other algorithms fail to execute. Performance comparison in terms of efficiency is QPSOVIC > CS > QPSO > PSO that is demonstrated from Table 5.1.
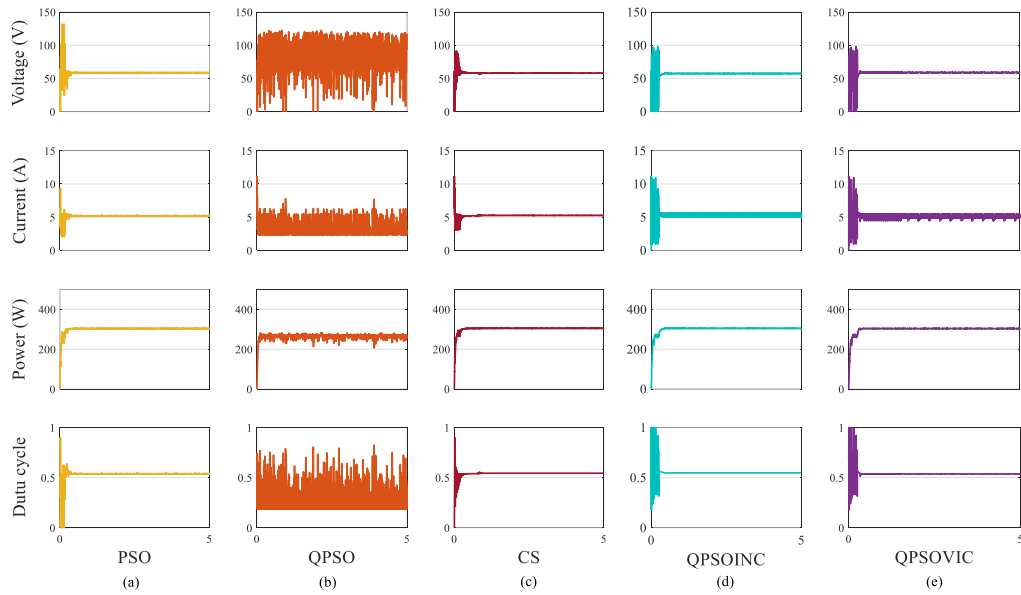
Figure 5.11 5 s simulation under 0U4P test condition for (a) PSO (b) QPSO (c) CS (d) QPSOINC (e) QPSOVIC
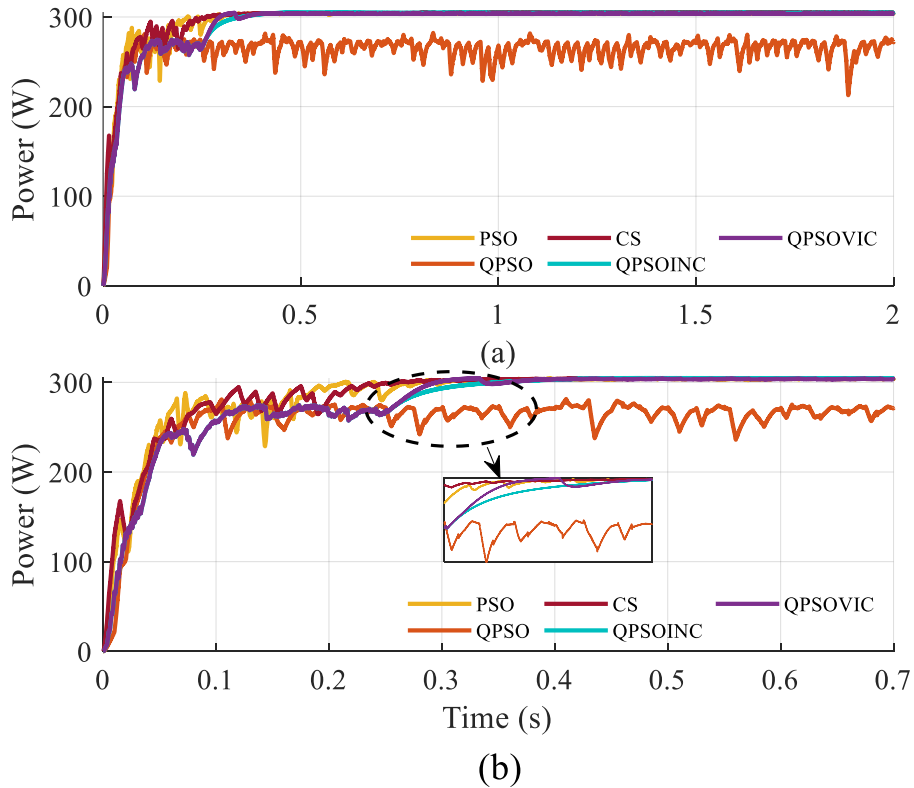
Figure 5.12 Power performance under 0U4P condition for (a) 5s (b) 0.6s (zoomed view)
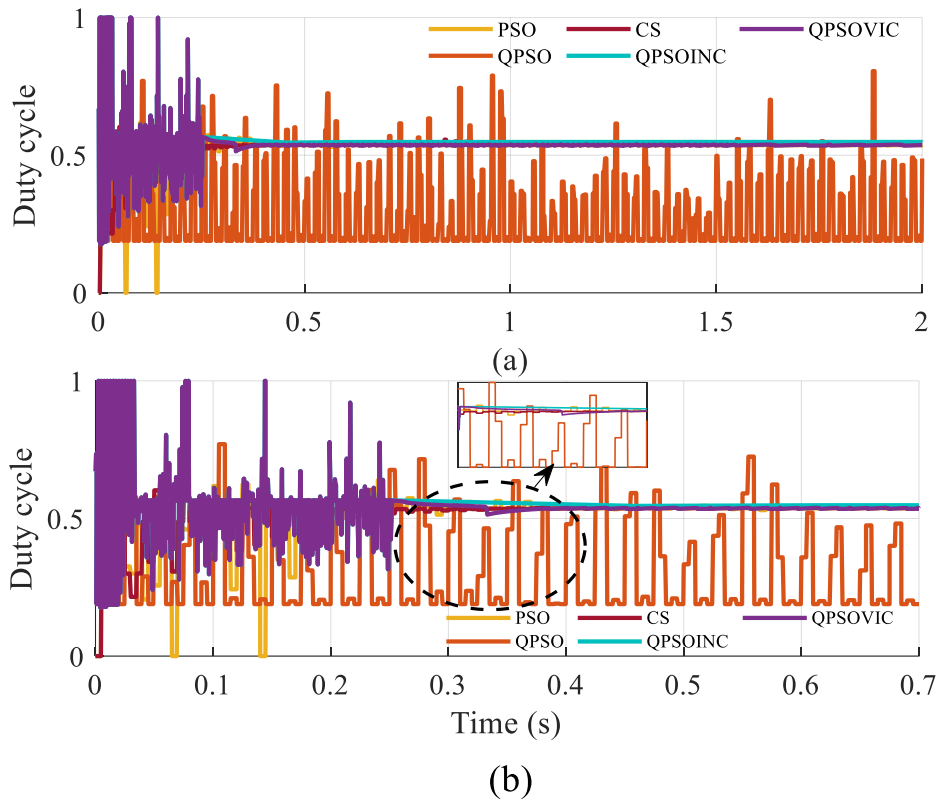
Figure 5.13 Duty Cycle under 0U4P condition for (a) 5s (b) 0.6s (zoomed view)

The performance indexes of PSO, QPSO, CS and QPSOVIC under all 4 test conditions have been summarized in the following table-

Table 5.1 Simulation result comparison

PV Configuration	Tracking Algorithm	Power (W)	Voltage (V)	Current (A)	Tracking time (S)	Maximum Power (W)	Efficiency (%)
4U0P	PSO	845.5	118.2	7.15	0.52	851.42	99.3
	QPSO	835.6	122.1	6.84	0.65		99.14
	CS	850.88	116.4	7.31	0.29		99.9
	QPSOINC	850.08	115.5	7.36	0.31		99.84
	QPSOVIC	851.4	116.06	7.3	0.29		99.99
2U2P	PSO	532.8	93.8	5.68	0.42	547.84	96.97
	QPSO	543.9	91.33	5.96	0.69		99.28
	CS	545.7	91.41	5.97	0.29		99.61
	QPSOINC	547.82	89.62	6.11	0.65		99.99
	QPSOVIC	547.83	90.08	6.08	0.33		99.99

	PSO	478.86	91.07	5.26	0.9		99.51
	QPSO	464.4	`93.69	4.96	0.5		96.51
1U3P	CS	481.14	90.44	5.32	0.26	481	99.98
	QPSOINC	481.13	90.22	5.33	0.3		99.98
	QPSOVIC	480.9	90.78	5.3	0.31		99.98
	PSO	268.7	-	-	-		88.14
	QPSO	302.7	58.83	5.14	0.54		99.29
0U4P	CS	304.2	58.47	5.2	0.3	304.84	99.79
	QPSOINC	304.7	57.36	5.31	0.43		99.95
	QPSOVIC	304.8	58.7	5.19	0.4		99.98

5.5   Varying irradiance Configuration:

In the final test case, we run all 4 different test conditions equipped with the QPSOVIC algorithm, where each of the test conditions change after 2.5s [Figure 5.14]. Using equation (25) $\Delta P(\%)$ is set to 15 to detect the change of irradiation and reinitializes the set of particles. First, the 4U0P test condition is observed from 0s to 2.5s, which converges to GMPP after 0.4s with a voltage reading of 116.4V, power is 851.3W and duty cycle is 0.45. Due to the IC algorithm the current at GMPP shows oscillations, the average value of current being 7.31A. After 2.5s the shaded condition changes to 2U2P and it ends at 5s. The convergence time is 0.48s and corresponding voltage is 89.9V, power is 546.2W, average current is 6.07A and duty cycle is 0.48. Test case 1U3P is observed from 5s to 7.5s. In this test case, the convergence time is higher than the other two test conditions taking 1.2s to converge to GMPP. At GMPP, the corresponding voltage is 90.06V, average current is 5.34A, power is 481.3W, and the duty cycle is 0.43. The last test case is 0U4P, which starts at 7.5s and ends at 10s. It takes about 2.17s to locate the GMPP which is higher compared to other test conditions. At GMPP, the corresponding voltage is 57.54V, average current is 5.29A, power is 304.9 W and the duty cycle is 0.546. The simultaneous changing of different test conditions proves the QPSOVIC's ability to seamlessly switch between any PSCs and track the GMPP efficiently and accurately.

Table 5.2 Qualitative comparison of the proposed algorithm

| Type	PSO	QPSO	CS	QPSOINC	QPSOVIC
Tracking speed	Average	Average	Vary fast	Fast	Fast
Transient power fluctuation	High	Average	Low	Low	Low
Tracking accuracy	Accurate	Very accurate	Very accurate	Very accurate	Very accurate
No. of tuning parameters	3	1	2	1	1
Steady state oscillations	Average	low	Zero	Zero	Zero
Power efficiency	High	High	High	High	High
Implementation complexity	Average	Average	Average	Average	Average
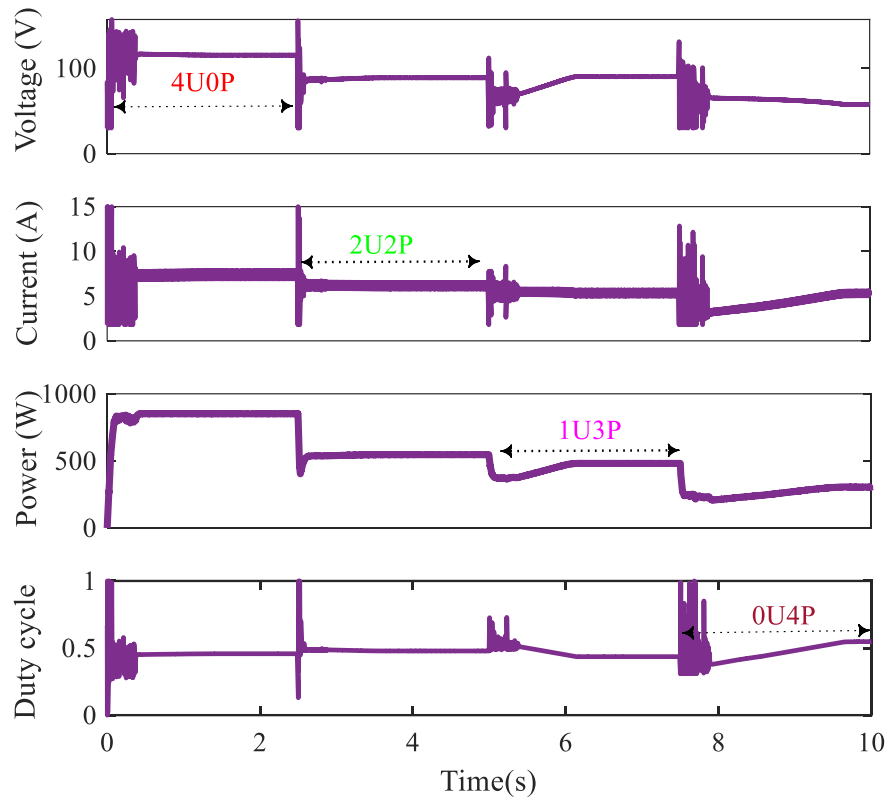
Figure 5.14 Performance of Hybrid QPSOVIC algorithm under fast varying test conditions
(4U0P > 2U2P > 1U3P > 0U4P)

Table 5.2 shows a quick comparison of the MPPT algorithms that have already been studied in terms of the performance indexes. Outcome of the simulation demonstrate that the optimal duty cycle is tracked effectively with small-scale oscillations utilizing the hybrid QPSOVIC method, resulting in minimal transient power fluctuation and above-average tracking characteristics compared to all of the other algorithms. From the table, it is also clear that in comparison with PSO and QPSO, the proposed algorithm provides better performance regarding accuracy, efficiency, steady-state error, and MPPT under extreme PSC also performs similar to the CS algorithm. Overall, the proposed QPSOVIC algorithm performs well in all the performance parameters.

Figure 5.15 shows the comparative analysis of the examined algorithms based on tracking time under various test settings. QPSOVIC shows superior tracking speed compared to the PSO and QPSO. The average efficiency has also been compared in Figure 5.16 where the QPSOVIC's performance is almost similar to the CS, both exhibiting higher efficiency than PSO and QPSO.
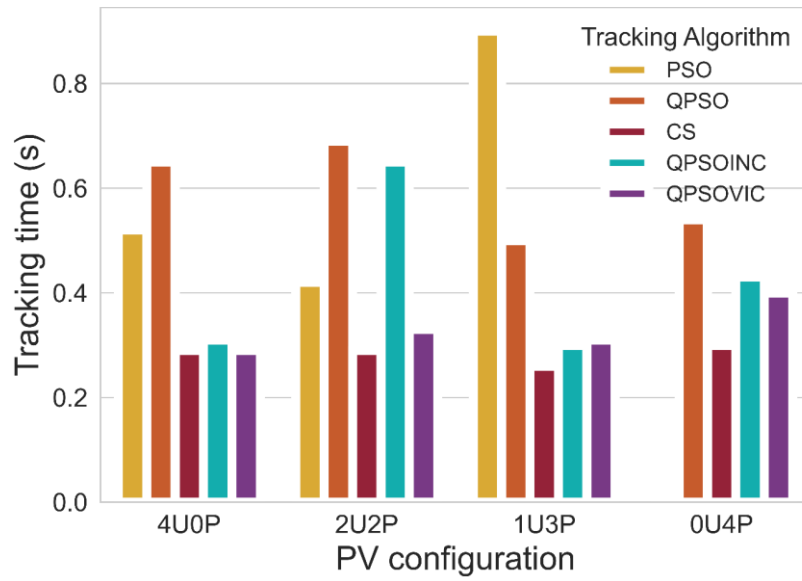
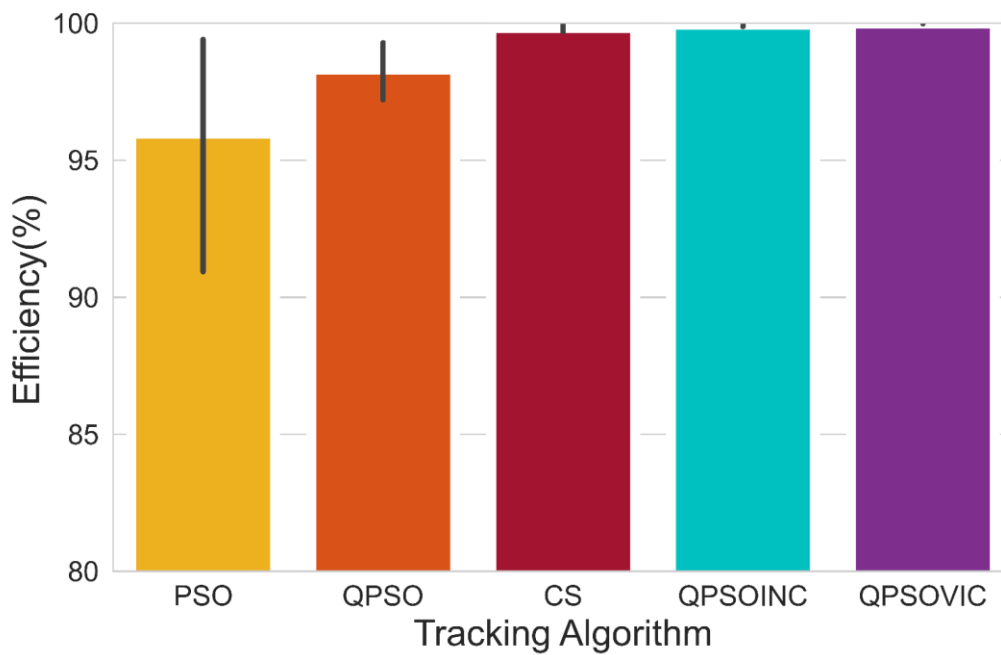**Figure 5.15** Tracking time of different test cases of different MPPT algorithms

Figure 5.16 Average efficiency of different MPPT algorithms

Chapter 6
Conclusion

6.1   Conclusion

A hybrid QPSOVIC algorithm is proposed in this paper that showed improved accuracy, reliability, and tracking speed under extreme PSCs. Four different partially shaded patterns are applied to the developed PV system equipped with the QPSOVIC. The simulation results prove the high efficiency and improved tracking speed of the QPSOVIC. In addition, it also shows the low transient power fluctuation and minimal steady-state oscillations. The proposed algorithm improves the MPPT by removing the random number coefficients and eliminating unnecessary iterations after the GMPP has been located. It uses the fast LMPP tracking ability of IC to leverage better tracking speed. Removing the extra tuning parameters may also make it simpler to implement using a low-cost microcontroller and mitigate complex tuning parameters of the PID controller.

6.2   Future Work and Scope

For future work, the system's physical implementation is yet to be explored. Originally our plan included hardware implementation which ultimately could not be executed due to the COVID-19 lockdown. The system implementation involves solar panels, a boost converter, a Raspberry Pi or PID controller, power supply to the controller, and signal conditioning circuits for the converters. Comparative analysis of the actual performance and the simulation will also be performed to determine the practicality of the proposed algorithm.

References

[1]   IRENA, *Renewable capacity statistics 2020 International Renewable Energy Agency*. 2020.

[2]   Z. Cheng, H. Zhou, and H. Yang, "Research on MPPT control of PV system based on PSO algorithm," *2010 Chinese Control Decis. Conf. CCDC 2010*, pp. 887–892, 2010, doi: 10.1109/CCDC.2010.5498097.

[3]   J. J. Nedumgatt, K. B. Jayakrishnan, S. Umashankar, D. Vijayakumar, and D. P. Kothari, "Perturb and observe MPPT algorithm for solar PV systems-modeling and simulation," *Proc. - 2011 Annu. IEEE India Conf. Eng. Sustain. Solut. INDICON-2011*, vol. 19, no. 1, 2011, doi: 10.1109/INDCON.2011.6139513.

[4]   A. Safari and S. Mekhilef, "Simulation and hardware implementation of incremental conductance MPPT with direct control method using cuk converter," *IEEE Trans. Ind. Electron.*, vol. 58, no. 4, pp. 1154–1161, 2011, doi: 10.1109/TIE.2010.2048834.

[5] M. I. Bahari, P. Tarassodi, Y. M. Naeini, A. K. Khalilabad, and P. Shirazi, "Algorithm For PhotoVoltaic Application," pp. 1041–1044, 2016.

[6] K. L. Lian, J. H. Jhang, and I. S. Tian, "A maximum power point tracking method based on perturb-and-observe combined with particle swarm optimization," *IEEE J. Photovoltaics*, vol. 4, no. 2, pp. 626–633, 2014, doi: 10.1109/JPHOTOV.2013.2297513.

[7] C. Sakthigokulrajan and K. Ravi, "Combined role of derived array configurations and MPSO based MPPT in improving the energy yield under partial shading conditions," *J. Build. Eng.*, vol. 9, no. July 2016, pp. 125–134, 2017, doi: 10.1016/j.jobe.2016.12.006.

[8] T. Radjai, L. Rahmani, S. Mekhilef, and J. P. Gaubert, "Implementation of a modified incremental conductance MPPT algorithm with direct control based on a fuzzy duty cycle change estimator using dSPACE," *Sol. Energy*, vol. 110, pp. 325–337, 2014, doi: 10.1016/j.solener.2014.09.014.

[9] K. S. Tey and S. Mekhilef, "Modified incremental conductance MPPT algorithm to mitigate inaccurate responses under fast-changing solar irradiation level," *Sol. Energy*, vol. 101, pp. 333–342, 2014, doi: 10.1016/j.solener.2014.01.003.

[10] K. S. Tey, S. Mekhilef, and S. Member, "Modified Incremental Conductance Algorithm for Photovoltaic System Under Partial Shading Conditions and Load Variation.pdf," vol. 61, no. 10, pp. 5384–5392, 2014.

[11] Z. Liying, M. Liang, L. Zhigang, C. Mingxuan, and W. Jianwen, "Implementation and simulation analysis of GMPPT algorithm under partial shadow condition," *Energy Procedia*, vol. 158, pp. 418–423, 2019, doi: 10.1016/j.egypro.2019.01.126.

[12] Y. Li, D. Ju, Y. Wang, J. E. Wu, and Z. Dong, "A global optimization method for multiple peak photovoltaic MPPT," *Proc. IECON 2017 - 43rd Annu. Conf. IEEE Ind. Electron. Soc.*, vol. 2017-Janua, pp. 554–559, 2017, doi: 10.1109/IECON.2017.8216097.

[13] S. Mohanty, B. Subudhi, and P. K. Ray, "A new MPPT design using grey Wolf optimization technique for photovoltaic system under partial shading conditions," *IEEE Trans. Sustain. Energy*, vol. 7, no. 1, pp. 181–188, 2016, doi: 10.1109/TSTE.2015.2482120.

[14] A. F. Mirza, M. Mansoor, Q. Ling, B. Yin, and M. Y. Javed, "A Salp-Swarm Optimization based MPPT technique for harvesting maximum energy from PV systems under partial shading conditions," *Energy Convers. Manag.*, vol. 209, no. October 2019, p. 112625, 2020, doi: 10.1016/j.enconman.2020.112625.

[15] S. Titri, C. Larbes, K. Y. Toumi, and K. Benatchba, "A new MPPT controller based on the Ant colony optimization algorithm for Photovoltaic systems under partial shading conditions," *Appl. Soft Comput. J.*, vol. 58, pp. 465–479, 2017, doi: 10.1016/j.asoc.2017.05.017.

[16] J. Ahmed and Z. Salam, "A Maximum Power Point Tracking (MPPT) for PV system using Cuckoo Search with partial shading capability," *Appl. Energy*, vol. 119, pp. 118–130, 2014, doi: 10.1016/j.apenergy.2013.12.062.

[17] D. P. Rini and S. M. Shamsuddin, "Particle Swarm Optimization: Technique, System and Challenges," *Int. J. Appl. Inf. Syst.*, vol. 1, no. 1, pp. 33–45, 2011, doi:

10.5120/ijais-3651.

[18] A. A. Zaki Diab and H. Rezk, "Global MPPT based on flower pollination and differential evolution algorithms to mitigate partial shading in building integrated PV system," *Sol. Energy*, vol. 157, pp. 171–186, 2017, doi: 10.1016/j.solener.2017.08.024.

[19] K. Sundareswaran, S. Peddapati, and S. Palani, "MPPT of PV systems under partial shaded conditions through a colony of flashing fireflies," *IEEE Trans. Energy Convers.*, vol. 29, no. 2, pp. 463–472, 2014, doi: 10.1109/TEC.2014.2298237.

[20] A. soufyane Benyoucef, A. Chouder, K. Kara, S. Silvestre, and O. A. Sahed, "Artificial bee colony based algorithm for maximum power point tracking (MPPT) for PV systems operating under partial shaded conditions," *Appl. Soft Comput. J.*, vol. 32, pp. 38–48, 2015, doi: 10.1016/j.asoc.2015.03.047.

[21] A. S. Oshaba, E. S. Ali, and S. M. Abd Elazim, "MPPT control design of PV system supplied SRM using BAT search algorithm," *Sustain. Energy, Grids Networks*, vol. 2, pp. 51–60, 2015, doi: 10.1016/j.segan.2015.04.002.

[22] M. S. Bouakkaz *et al.*, "Dynamic performance evaluation and improvement of PV energy generation systems using Moth Flame Optimization with combined fractional order PID and sliding mode controller," *Sol. Energy*, vol. 199, no. February, pp. 411–424, 2020, doi: 10.1016/j.solener.2020.02.055.

[23] A. M. Eltamaly, M. S. Al-Saud, and A. G. Abo-Khalil, "Performance improvement of PV systems' maximum power point tracker based on a scanning PSO particle strategy," *Sustain.*, vol. 12, no. 3, pp. 1–20, 2020, doi: 10.3390/su12031185.

[24] J. Shi, W. Zhang, Y. Zhang, F. Xue, and T. Yang, "MPPT for PV systems based on a dormant PSO algorithm," *Electr. Power Syst. Res.*, vol. 123, pp. 100–107, 2015, doi: 10.1016/j.epsr.2015.02.001.

[25] A. M. Eltamaly, H. M. H. Farh, and A. G. Abokhalil, "A novel PSO strategy for improving dynamic change partial shading photovoltaic maximum power point tracker," *Energy Sources, Part A Recover. Util. Environ. Eff.*, 2020, doi: 10.1080/15567036.2020.1769774.

[26] P. S. Gavhane, S. Krishnamurthy, R. Dixit, J. P. Ram, and N. Rajasekar, "EL-PSO based MPPT for Solar PV under Partial Shaded Condition," *Energy Procedia*, vol. 117, pp. 1047–1053, 2017, doi: 10.1016/j.egypro.2017.05.227.

[27] K. Ishaque, Z. Salam, H. Taheri, and A. Shamsudin, "Maximum Power Point Tracking for PV system under partial shading condition via particle swarm optimization," *2011 IEEE Appl. Power Electron. Colloquium, IAPEC 2011*, vol. 2, no. 2, pp. 5–9, 2011, doi: 10.1109/IAPEC.2011.5779866.

[28] M. GREEN *et al.*, "Solar cell efficiency tables (version 40)," *Ieee Trans Fuzzy Syst*, vol. 20, no. 6, pp. 1114–1129, 2012, doi: 10.1002/pip.

[29] Y. Zou, Y. Yu, Y. Zhang, and J. Lu, "MPPT control for PV generation system based on an improved IncCond algorithm," *Procedia Eng.*, vol. 29, pp. 105–109, 2012, doi: 10.1016/j.proeng.2011.12.677.

[30] M. Abdulkadir and A. H. M. Yatim, "Hybrid maximum power point tracking technique based on PSO and incremental conductance," *2014 IEEE Conf. Energy Conversion, CENCON 2014*, pp. 271–276, 2014, doi: 10.1109/CENCON.2014.6967514.

[31] H. Bellia, R. Youcef, and M. Fatima, "A detailed modeling of photovoltaic module using MATLAB," *NRIAG J. Astron. Geophys.*, vol. 3, no. 1, pp. 53–61, 2014, doi: 10.1016/j.nrjag.2014.04.001.

[32] H. Ibrahim and N. Anani, "Variations of PV module parameters with irradiance and temperature," *Energy Procedia*, vol. 134, pp. 276–285, 2017, doi: 10.1016/j.egypro.2017.09.617.

[33] Iw. Christopher and S. Assistant Professor, "Comparative Study of P&O and InC MPPT Algorithms," *Am. J. Eng. Res.*, vol. 02, no. 12, pp. 402–408, 2013, [Online]. Available: www.ajer.org.

[34] R. B. A. Koad and A. F. Zobaa, "Comparison between the Conventional Methods and PSO Based MPPT Algorithm for Photovoltaic Systems," *Int. J. Electr. Robot. Electron. Commun. Eng.*, vol. 8, no. 4, pp. 673–678, 2014, doi: 10.5281/zenodo.1092094.

[35] N. Rajasekar *et al.*, "Application of modified particle swarm optimization for maximum power point tracking under partial shading condition," *Energy Procedia*, vol. 61, pp. 2633–2639, 2014, doi: 10.1016/j.egypro.2014.12.265.

[36] M. Mansoor, A. F. Mirza, Q. Ling, and M. Y. Javed, "Novel Grass Hopper optimization based MPPT of PV systems for complex partial shading conditions," *Sol. Energy*, vol. 198, no. January, pp. 499–518, 2020, doi: 10.1016/j.solener.2020.01.070.

[37] L. A. Soriano, P. Ponce, and A. Molina, "Analysis of DC-DC converters for photovoltaic applications based on conventional MPPT algorithms," *2017 14th Int. Conf. Electr. Eng. Comput. Sci. Autom. Control. CCE 2017*, 2017, doi: 10.1109/ICEEE.2017.8108884.

[38] X. Yang, S. Deb, and A. C. B. Behaviour, "Cuckoo Search via L´evy Flights," *Ieee*, pp. 210–214, 2009.

[39] Y. Teuschl, B. Taborsky, and M. Taborsky, "How do cuckoos find their hosts? The role of habitat imprinting," *Anim. Behav.*, vol. 56, no. 6, pp. 1425–1433, 1998, doi: 10.1006/anbe.1998.0931.

[40] X. S. Yang and S. Deb, "Multiobjective cuckoo search for design optimization," *Comput. Oper. Res.*, vol. 40, no. 6, pp. 1616–1624, 2013, doi: 10.1016/j.cor.2011.09.026.

[41] P. Mohanty, G. Bhuvaneswari, R. Balasubramanian, and N. K. Dhaliwal, "MATLAB based modeling to study the performance of different MPPT techniques used for solar PV system under various operating conditions," *Renew. Sustain. Energy Rev.*, vol. 38, pp. 581–593, 2014, doi: 10.1016/j.rser.2014.06.001.

[42] J. Sun, W. Xu, and B. Feng, "A global search strategy of Quantum-behaved Particle Swarm Optimization," *2004 IEEE Conf. Cybern. Intell. Syst.*, pp. 111–116, 2004, doi: 10.1109/iccis.2004.1460396.

[43] C. M. K. James, "The Particle Swarm—Explosion, Stability, and Convergence in a Multidimensional Complex Space," *Mutat. Res. DNAging*, vol. 275, no. 1, pp. 1–6, 1992, doi: 10.1016/0921-8734(92)90002-7.

[44] S. Chen, "Quantum-behaved particle swarm optimization with weighted mean personal best position and adaptive local attractor," *Inf.*, vol. 10, no. 1, 2019, doi: 10.3390/info10010022.

[45]   D. Pilakkat and S. Kanthalakshmi, "An improved P&O algorithm integrated with artificial bee colony for photovoltaic systems under partial shading conditions," *Sol. Energy*, vol. 178, no. December 2018, pp. 37–47, 2019, doi: 10.1016/j.solener.2018.12.008.

[46]   F. Liu, S. Duan, F. Liu, B. Liu, and Y. Kang, "A variable step size INC MPPT method for PV systems," *IEEE Trans. Ind. Electron.*, vol. 55, no. 7, pp. 2622–2628, 2008, doi: 10.1109/TIE.2008.920550.

[47]   Q. Mei, M. Shan, L. Liu, and J. M. Guerrero, "A novel improved variable step-size incremental-resistance MPPT method for PV systems," *IEEE Trans. Ind. Electron.*, vol. 58, no. 6, pp. 2427–2434, 2011, doi: 10.1109/TIE.2010.2064275.

[48]   E. M. Ahmed and M. Shoyama, "Novel stability analysis of variable step size incremental resistance INR MPPT for PV systems," *IECON Proc. (Industrial Electron. Conf.*, pp. 3894–3899, 2011, doi: 10.1109/IECON.2011.6119945.

[49]   N. H. Abdul Rahman, A. M. Omar, and E. H. Mat Saat, "A modification of variable step size INC MPPT in PV system," *Proc. 2013 IEEE 7th Int. Power Eng. Optim. Conf. PEOCO 2013*, no. June, pp. 340–345, 2013, doi: 10.1109/PEOCO.2013.6564569.

[50]   A. Stracke, D. L. Danielopol, and W. Neubauer, "Comparative study of MPPT using variable step size for photovoltaic systems," *2014 Second World Conf. Complex Syst.*, vol. 2008, no. 3, pp. 83–88, 2008.

[51]   C. Li, Y. Chen, D. Zhou, J. Liu, and J. Zeng, "A high-performance adaptive incremental conductance MPPT algorithm for photovoltaic systems," *Energies*, vol. 9, no. 4, 2016, doi: 10.3390/en9040288.

[52]   S. Mohanty, B. Subudhi, and P. K. Ray, "A Grey Wolf-Assisted Perturb & Observe MPPT Algorithm for a PV System," *IEEE Trans. Energy Convers.*, vol. 32, no. 1, pp. 340–347, 2017, doi: 10.1109/TEC.2016.2633722.

[53]   B. N. Alajmi, K. H. Ahmed, S. J. Finney, and B. W. Williams, "A maximum power point tracking technique for partially shaded photovoltaic systems in microgrids," *IEEE Trans. Ind. Electron.*, vol. 60, no. 4, pp. 1596–1606, 2013, doi: 10.1109/TIE.2011.2168796.